

Four-Loop Renormalisation of Chiral Gauge Theories with Non-Anticommuting γ_5 in the BMHV Scheme

Andreas von Manteuffel,^{a*} Dominik Stöckinger,^{b†} Matthias Weißwange,^{b‡}

^aInstitut für Theoretische Physik, Universität Regensburg,
Universitätstraße 31, DE-93040 Regensburg, Germany

^bInstitut für Kern- und Teilchenphysik, TU Dresden,
Zellescher Weg 19, DE-01069 Dresden, Germany

17th June 2025

Abstract

We present the complete 4-loop renormalisation of an Abelian chiral gauge theory in the Breitenlohner-Maison / 't Hooft-Veltman (BMHV) scheme. Employing a non-anticommuting γ_5 in dimensional regularisation, we determine the full set of symmetry restoring counterterms from the quantum action principle. Our calculation represents the highest-order application of the BMHV framework so far, pushing the limits of a self-consistent treatment of γ_5 at the multi-loop level. We describe the computational setup that we developed to perform the computations and discuss key implementation aspects, such as the BMHV algebra and tensor reduction. Our work demonstrates the feasibility of applying the BMHV scheme at high loop orders and establishes a solid foundation for future studies of high-precision electroweak physics.

*manteuffel@ur.de

†dominik.stoeckinger@tu-dresden.de

‡matthias.weisswange@tu-dresden.de

Contents

1	Introduction	2
2	Abelian Chiral Gauge Theory in the BMHV Scheme	3
3	Computational Setup and Methods	4
3.1	Computational Setup	4
3.2	BMHV-Specific Challenges	6
3.3	BMHV Algebra with Non-Anticommuting γ_5	9
3.4	Tadpole Decomposition	10
3.5	Practical Implementation of Counterterms	12
3.6	Tensor Reduction	13
4	Four-Loop Renormalisation	18
4.1	Four-Loop Singular Counterterm Action	19
4.2	Four-Loop BRST Breaking	20
4.3	Four-Loop Finite Symmetry-Restoring Counterterms	22
4.4	Application to the Abelian Fermionic Sector of the SM	23
5	Conclusions	24
	Appendices	25
A	Derivation of the γ-Trace Factorisation in D Dimensions	26
B	Explicit Results for the Four-Loop Coefficients	27

1 Introduction

Chiral gauge theories play a central role in the Standard Model (SM) and beyond, yet their consistent treatment represents a long-standing challenge due to the well-known γ_5 -problem. In Dimensional Regularisation (DReg), the Breitenlohner-Maison/'t Hooft-Veltman (BMHV) scheme, see Refs. [1–4] and Refs. [5, 6] for reviews, provides the only known way for a mathematically consistent treatment of γ_5 . In particular, γ_5 remains manifestly 4-dimensional in the BMHV scheme of DReg, while anticommutativity with the fully D -dimensional γ^μ -matrices is abandoned. This results in modified algebraic relations and ultimately in a violation of gauge and BRST invariance. Hence, consistency comes at the cost of a regularisation-induced symmetry breaking, which must be restored in the course of renormalisation. This leads to an increased computational effort, which becomes particularly significant in multi-loop applications.

In order to avoid this symmetry breaking, different γ_5 -schemes have been proposed. For example, “Kreimer’s scheme”, Refs. [7–9], abandons the cyclicity of γ -traces, while “Larin’s prescription”, Ref. [10], suggests a treatment for axial currents in specific applications. However, none of these approaches constitutes a fully self-consistent scheme that is free of ambiguities. In particular, their scope of application at the multi-loop level is limited and not entirely under control, as demonstrated in e.g. Refs. [11–19]. Therefore, we adopt a no-compromise approach to the treatment of γ_5 within the BMHV scheme.

The BMHV scheme has been studied at the 1-loop level in non-Abelian chiral gauge theories with and without scalar fields in Refs. [20, 21], and [22, 23], respectively, and in the Abelian Higgs model in Ref. [24]. A general Abelian chiral gauge theory with scalars as well as different choices for evanescent gauge interactions and dimensionally regularised fermions was analysed at the 1-loop level in Ref. [25]. Recent applications of the BMHV scheme to effective field theories can be found in Refs. [26–30]. In Abelian theories, the BMHV scheme has thoroughly been studied at higher orders, with a 2-loop application in Refs. [31, 32] and an extension to the 3-loop level in Ref. [33]. For non-Abelian theories, a full 2-loop renormalisation is presented in Ref. [34], with initial discussions in Ref. [35].

The intricacies of the γ_5 -problem as well as inconsistencies of other γ_5 -schemes that emerge at the multi-loop level render the multi-loop properties of the BMHV scheme highly relevant. In this work, we present the first 4-loop application of the BMHV scheme, marking the highest-order calculation performed within this framework and pushing the limits of our approach to symmetry restoration, see Refs. [20, 25, 31, 33, 35]. This approach is based on the quantum action principle of DReg, see Ref. [4] and Ref. [6] for a review. In particular, this work directly extends previous studies in Refs. [31, 33]. Performing such multi-loop calculations requires an efficient computational framework. To address these challenges, we developed a completely new computational setup, where most computationally expensive operations are carried out in FORM [36–38]. This significantly enhances computational performance, enabling not only the current 4-loop calculation, which involves billions of terms in intermediate steps, but also future SM applications.

This paper is organised as follows: In Sec. 2, we introduce the Abelian chiral gauge theory considered in this work. In Sec. 3, we discuss our computational setup and the methods used to obtain our results, including the implementation of the BMHV algebra, the tadpole decomposition for extracting UV divergences, and the tensor reduction. In Sec. 4, we present our results for the 4-loop renormalisation of the model under consideration, including the explicit symmetry restoration. Finally, we conclude in Sec. 5.

2 Abelian Chiral Gauge Theory in the BMHV Scheme

In this paper, we consider a chiral gauge theory of right-handed fermions ψ_{Ri} interacting with the Abelian gauge boson B^μ via the hypercharge matrix \mathcal{Y}_R . The theory is regularised using DReg and the BMHV scheme for the treatment of γ_5 . The tree-level action S_0 of this theory is defined via the following D -dimensional tree-level Lagrangian

$$\mathcal{L} = \mathcal{L}_{\text{fermion}} + \mathcal{L}_{\text{gauge}} + \mathcal{L}_{\text{ghost+fix}} + \mathcal{L}_{\text{ext}}. \quad (2.1)$$

For properly regularised loop-diagrams, we require D -dimensional fermion kinetic terms. In the present case, this means that we need to introduce fictitious, sterile¹ left-handed partner fields ψ_{Li}^{st} for each fermion, such that we can construct Dirac spinors of the form $\psi_i = \psi_{Li}^{\text{st}} + \psi_{Ri}$.² In this way the fermion kinetic terms read

$$\mathcal{L}_{\text{kin,f}} = \bar{\psi}_j i \not{\partial} \psi_j = \bar{\psi}_{Rj} i \not{\partial} \psi_{Rj} + \bar{\psi}_{Lj}^{\text{st}} i \not{\partial} \psi_{Lj}^{\text{st}} + \bar{\psi}_{Rj} i \widehat{\not{\partial}} \psi_{Lj}^{\text{st}} + \bar{\psi}_{Lj}^{\text{st}} i \widehat{\not{\partial}} \psi_{Rj}, \quad (2.2)$$

where all D -dimensional quantities have been split into purely 4-dimensional and remaining $(D-4)$ -dimensional parts as e.g. $\gamma^\mu = \bar{\gamma}^\mu + \widehat{\gamma}^\mu$, such that the modified BMHV commutation relations with γ_5 are $\{\bar{\gamma}^\mu, \gamma_5\} = [\widehat{\gamma}^\mu, \gamma_5] = 0$, see Sec. 3.3 for further details. Clearly, an inevitable consequence of this modified algebra is the mixing of chiralities in the last two terms of Eq. (2.2), i.e. in the evanescent part of the fermion kinetic term. Including the gauge boson interaction with the physical fermions, the full fermionic Lagrangian is

$$\mathcal{L}_{\text{fermion}} = \bar{\psi}_j i \not{\partial} \psi_j - g \mathcal{Y}_{Rij} \bar{\psi}_i \not{B} \psi_j, \quad (2.3)$$

where the hypercharge matrix satisfies the anomaly cancellation condition

$$\text{Tr}(\mathcal{Y}_R^3) \equiv 0. \quad (2.4)$$

The mismatch between the purely 4-dimensional and right-handed gauge interaction in Eq. (2.3) and the fully D -dimensional kinetic term including the resulting mixing of left- and right-handed fermions with different gauge quantum numbers causes the violation of gauge and BRST invariance — the main drawback of the BMHV scheme. For more information regarding this issue, we refer the reader to Refs. [6, 20, 31, 33, 35] and in particular to Ref. [25] for a detailed analysis concerning the treatment of fermions in D dimensions in the context of the BMHV scheme. For the gauge boson, we have

$$\mathcal{L}_{\text{gauge}} = -\frac{1}{4} F^{\mu\nu} F_{\mu\nu}, \quad (2.5)$$

with field strength tensor $F_{\mu\nu} = \partial_\mu B_\nu - \partial_\nu B_\mu$. The familiar R_ξ -gauge fixing and the Abelian ghosts enter the D -dimensional Lagrangian via

$$\mathcal{L}_{\text{ghost+fix}} = -\frac{1}{2\xi} (\partial^\mu B_\mu)^2 - \bar{c} \square c. \quad (2.6)$$

Finally, in order to work with Slavnov-Taylor identities, along with the quantum action principle of DReg, we are required to couple the BRST transformations of the fields

$$s_D B_\mu(x) = \partial_\mu c(x), \quad s_D \psi_{Ri}(x) = -igc(x) \mathcal{Y}_{R,ij} \psi_{Rj}(x), \quad s_D c(x) = 0, \quad (2.7)$$

¹Sterile fields do not participate in any interaction.

²Here, this is our only option, as the theory contains no physical left-handed fermions.

to external sources $\{\rho^\mu, R^i, \zeta\}$ and take them into account via

$$\mathcal{L}_{\text{ext}} = \rho^\mu s_D B_\mu + \bar{R}^i s_D \psi_{R_i} + (s_D \bar{\psi}_{R_i}) R^i + \zeta s_D c, \quad (2.8)$$

where s_D denotes the D -dimensional BRST operator. The aforementioned regularisation induced symmetry breaking is then explicitly given by

$$\widehat{\Delta} \equiv s_D S_0 = -g \mathcal{Y}_{R,ij} \int d^D x c \left\{ \bar{\psi}_i \left(\overleftarrow{\widehat{\partial}} \mathbb{P}_R + \overrightarrow{\widehat{\partial}} \mathbb{P}_L \right) \psi_j \right\} = \int d^D x \widehat{\Delta}(x). \quad (2.9)$$

The goal of the present paper is to determine the 4-loop renormalisation of the model. This requires the computation of power-counting divergent Green functions at the 4-loop level. The set of Green functions consists of standard Green functions with physical external fields and Green functions with insertions of the composite operator Δ and external Faddeev-Popov ghost c .

3 Computational Setup and Methods

In this section, we present the computational setup used for all calculations in this project and discuss the methods employed. These methods and our implementation are applicable to various models; thus, we keep the discussion largely model-independent, while illustrating certain aspects and challenges, where appropriate, with the help of the specific theory introduced in Sec. 2.

We begin with a concise overview of our workflow, including the software tools utilised, and highlight major challenges specific to calculations involving non-anticommuting γ_5 in the BMHV scheme of DReg. Next, we discuss the so-called BMHV algebra and provide implementation details in FORM within our setup. We then outline our approach for extracting UV divergences using a tadpole decomposition and describe the implementation of counterterms. Finally, we explain our tensor reduction procedure along with its implementation.

3.1 Computational Setup

To calculate Green functions, we generate Feynman diagrams with QGRAF [39] and process its output with a sequence of FORM programs. We start this sequence by inserting the Feynman rules into the diagram to obtain an expression for the multi-leg Green function. Since we wish to extract its UV divergences, we apply a tadpole decomposition to map all Feynman integrals to fully massive, single scale vacuum bubbles. Details for this step are given below in Sec. 3.4.

Our goal is to express the resulting vacuum bubbles in terms of scalar integrals according to

$$I(\nu_1, \dots, \nu_N) = (\mu^{4-D})^L \int \left(\prod_{i=1}^L \frac{d^D k_i}{(2\pi)^D} \right) \frac{1}{\mathcal{D}_1^{\nu_1} \dots \mathcal{D}_N^{\nu_N}}, \quad (3.1)$$

where L denotes the loop-order, $D = 4 - 2\epsilon$ is the spacetime dimension, and $N = N(L) = L(L+1)/2$ is the number of different propagators for vacuum bubbles without external momenta. Here, the propagators are of the form

$$\mathcal{D}_i = q_i^2 - M^2, \quad (3.2)$$

	B_1	B_2	B_3	B_4
q_1	k_1	k_1	k_1	k_1
q_2		k_2	k_2	k_2
q_3		$k_1 - k_2$	k_3	k_3
q_4			$k_1 - k_2$	k_4
q_5			$k_1 - k_3$	$k_1 - k_4$
q_6			$k_2 - k_3$	$k_2 - k_4$
q_7				$k_3 - k_4$
q_8				$k_1 - k_2$
q_9				$k_1 - k_3$
q_{10}				$k_1 - k_2 - k_3$

Table 1: Propagator momenta q_i for fully massive single scale vacuum bubbles up to $L = 4$ loops, see Ref. [40].

where q_i is a linear combination of loop momenta. For each loop order considered in this paper, a single choice of propagator momentum configurations

$$B_L = \left\{ q_i \mid i \in \{1, \dots, N(L)\}; \{q_i^2\} \text{ linearly independent} \right\} \quad (3.3)$$

is sufficient to cover all Feynman diagrams. Here, we adopt the convention of Ref. [40], with propagator momenta shown in Tab. 1.

Due to ambiguities in the assignment of loop momenta, the momenta encountered in the denominators of our diagrams do not automatically match those of the chosen integral families. To achieve this, we employ the program `Feynson` [41], which systematically shifts loop momenta such that only the momentum configurations listed in Tab. 1 appear in the denominators of the Feynman integrals.

At this stage of the calculation, we usually encounter tensor integrals that are not of the form (3.1) due to loop momenta with open Lorentz indices in the numerator. To address this, we apply a tensor reduction which expresses tensor integrals in terms of scalar integrals $I(\nu_1, \dots, \nu_N)$ defined by Eq. (3.1). Since tensor reduction is among the most computationally expensive steps of the calculation, we have implemented an efficient tensor reduction procedure in `FORM`, which is explained in Sec. 3.6.

Following the tensor reduction, we perform the Dirac algebra. Specifically, we employ a non-anticommuting γ_5 in the framework of the BMHV scheme. For this purpose, we have implemented a dedicated `FORM` procedure that efficiently applies the BMHV algebra while leveraging as many built-in `FORM` operations as possible. A corresponding discussion of this procedure is to be found in Sec. 3.3.

As a final step of the calculation, the general scalar integrals $I(\nu_1, \dots, \nu_N)$ are reduced to a finite set of master integrals using integration-by-parts (IBP) identities. For this purpose, we employ the C++ version of `FIRE` [42, 43]. To ensure that `FIRE` reduces all integrals to a minimal set of preferred master integrals, we additionally use `Reduze2` [44] to identify and generate sector symmetry relations, which is particularly crucial at the 4-loop level. We also employed `Kira` [45–48] and the private code `Finred` based on finite field arithmetic [49–51] for cross checks and basis changes. The solutions for the master integrals at the 2- and 3-loop level have been taken from Refs. [52, 53], while the 4-loop master integrals have been obtained from Ref. [54].

In our new computational setup, we employ `Mathematica` [55] only to interface various software tools and for the automated generation of `FORM` code. All performance-relevant operations are carried out in carefully optimised `FORM` programs and dedicated IBP solvers, removing a major bottleneck encountered in past calculations, cf. Refs. [33, 35].

The setup described above has successfully been tested and applied up to the 4-loop level. We performed a complete renormalisation of ordinary vector-like quantum electrodynamics (QED) at the 4-loop level and validated our results against the literature. Additionally, we successfully reproduced our previous results for the Abelian chiral gauge theory considered here up to the 3-loop level, see Refs. [31, 33].

3.2 BMHV-Specific Challenges

In this subsection, we highlight two major challenges specific to calculations in chiral gauge theories within the BMHV scheme, which increase the computational effort compared to vector-like gauge theories. These challenges arise due to the regularisation-induced symmetry breaking and the modified algebraic relations responsible for this breaking, details for which will be given in Sec. 3.3 below. To illustrate these challenges, we briefly contrast ordinary vector-like QED (regularised using naive DReg) with the Abelian chiral gauge theory studied in this work (regularised in the BMHV scheme of DReg), using explicit examples of Green functions and Feynman diagrams. Afterwards, we comment on the implications for the computation of physical observables and emphasise that, despite these challenges, the BMHV scheme remains of practical relevance. The two primary computational challenges in the BMHV scheme are:

- (i) Ward and Slavnov-Taylor identities are broken, preventing their usage.
- (ii) More Lorentz covariants occur, involving both D -dimensional and $(D-4)$ -dimensional indices.

The first issue implies that Ward or Slavnov-Taylor identities cannot be used to circumvent the computation of multi-leg (≥ 3) 1PI Green functions, as is typically done (see e.g. [12, 15–17, 56–59]). Consequently, for a complete renormalisation of a given chiral gauge theory in the BMHV scheme at a given loop order, 1PI Green functions with up to five external legs must be calculated, see Refs. [25, 34]. In the Abelian chiral gauge theory considered here, we need to take Green functions with up to four external legs into account, see Sec. 4.1 and 4.2. Clearly, this significantly increases the total number of 1PI Green functions required for a complete renormalisation.

The second issue concerns the proliferation of Lorentz covariants. On the one hand, it is necessary to compute multi-leg (≥ 3) 1PI Green functions due to symmetry breaking, cf. (i), leading to more complicated Lorentz structures. This issue is evident not only in previous results, Refs. [6, 20, 25, 31, 33, 35], but also in the present results in Sec. 4. On the other hand, the BMHV algebra leads to both D -dimensional and $(D-4)$ -dimensional Lorentz indices. Our goal is to work with standard, scalar Feynman integrals. In ordinary vector-like QED one could simply employ projectors at the level of Green functions and contract Lorentz indices to achieve this. Here, instead, we wish to avoid the contraction of loop momenta with non- D -dimensional indices resulting from the evaluation of the BMHV Dirac algebra, as this can generate 4- and $(D-4)$ -dimensional loop momentum numerator polynomials. We solve this problem by performing a D -dimensional tensor reduction of

the tensor integrals. Since we encounter high tensor ranks, our tensor reduction procedure needs to be highly efficient.

As an alternative to tensor reduction as used in this work, one could employ a method to deal with $(D - 4)$ dimensional scalar products of the form $\widehat{k}_i \cdot \widehat{k}_j$ in the numerators of the loop integrals, also known as “ μ -terms”. These non-standard loop integrals can not directly be processed by standard IBP solvers and their solutions are not readily available. They thus require a dedicated treatment. At 1- and 2-loop order, a suitable method has been discussed in Refs. [60, 61] already some time ago. A review and an application at 2-loops was presented in Ref. [62]. At higher loop orders, no such method has been worked out yet. In this paper, we do not consider this option any further and strictly insist on purely D -dimensional loop integrals.

To summarise, the renormalisation of chiral gauge theories requires a significantly higher computational effort compared to vector-like gauge theories. This is not only due to the increased number of required Green functions, but also because each Green function involves higher computational complexity. Moreover, the regularisation-induced violation of gauge and BRST invariance necessitates the determination of finite, symmetry-restoring counterterms. These can be derived from 1PI Green functions with an insertion of a local composite operator Δ that encodes the symmetry breaking, see Sec. 4.2 for a brief illustration of our methodology. Although this symmetry-restoration procedure is highly efficient, it still requires the computation of additional Green functions.

In the following we illustrate these challenges by comparing the renormalisation of ordinary vector-like QED and that of the Abelian chiral gauge theory studied here, see Sec. 2. In vector-like QED, Ward identities ensure that it is sufficient to compute only the self-energies of the gauge boson and the fermions in order to obtain all renormalisation constants. In contrast, the Abelian chiral gauge theory, regularised in the BMHV scheme, requires the computation of five standard Green functions and four Green functions with the insertion of a local composite operator Δ . The required Green functions will be listed below in Eqs. (4.3)-(4.7) as well as Eqs. (4.24)-(4.27), and involve e.g. four-point functions $B^\mu B^\nu B^\rho B^\sigma$ and $cB^\mu B^\nu B^\rho$ as well as an unusual 2-point function cB^μ , where c is the Faddeev-Popov ghost. Among these, the Δ -inserted Green functions associated to cB^μ and $cB^\mu B^\nu B^\rho$ are particularly computationally expensive. Both involve rank-12 tensor integrals at the 4-loop level. The cB^μ Green function additionally has a superficial degree of divergence of 3, which leads to a large number of terms after tadpole decomposition, see Sec. 3.4. Two representative 4-loop diagrams for this Green function are shown in Fig. 1. The 4-point Green function $cB^\mu B^\nu B^\rho$, while having a comparatively low degree of divergence of 1, involves a significantly larger number Feynman diagrams, see Fig. 2 for two 4-loop representatives. All of these diagrams involve the insertion of $\widehat{\Delta}$, see Eq. (2.9), which corresponds to the tree-level contribution of the composite operator Δ .

The BMHV scheme does not introduce additional tree-level vertices which could enter standard Green functions (without Δ -insertions). Hence, at the L -loop level, the number of genuine L -loop diagrams in standard Green functions is the same as in other regularisation schemes. For example, the 1PI Green functions associated to $B^\mu B^\nu$, $\overline{\psi}\psi$, $\overline{\psi}B^\mu\psi$ and $B^\mu B^\nu B^\rho B^\sigma$ contain the same number of genuine L -loop diagrams in both vector-like QED and the BMHV-regularised Abelian chiral gauge theory. However, symmetry-restoring counterterms lead to additional ($< L$)-loop counterterm-inserted diagrams. Moreover, since the breaking Δ itself receives loop corrections, further ($< L$)-loop counterterm-inserted diagrams arise from these higher-order contributions. Fig. 3 shows two repres-

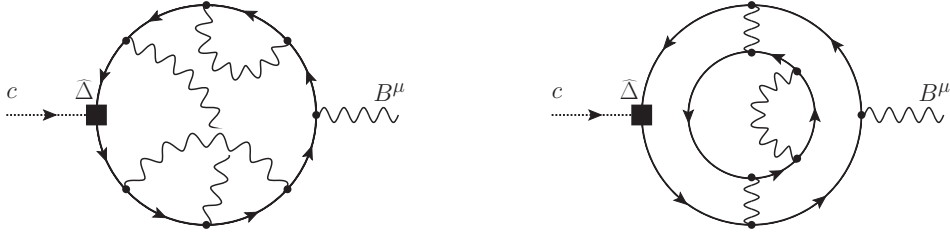


Figure 1: Representative 4-loop Feynman diagrams contributing to the Δ -operator-inserted 1PI Green function $i\Delta \cdot \Gamma|_{B_\mu c}^4$.

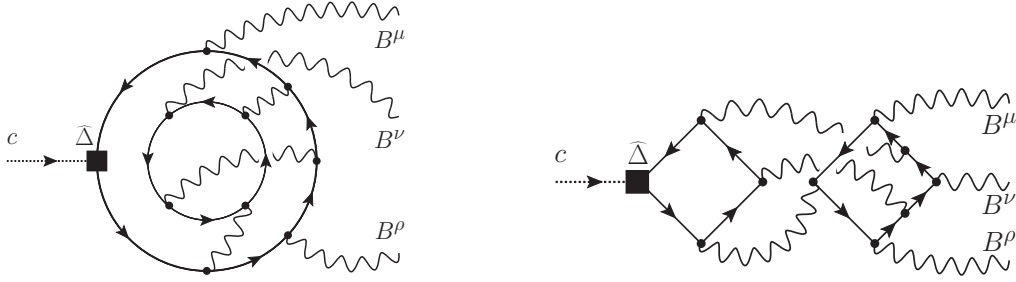


Figure 2: Representative 4-loop Feynman diagrams contributing to the Δ -operator-inserted 1PI Green function $i\Delta \cdot \Gamma|_{B_\rho B_\nu B_\mu c}^4$.

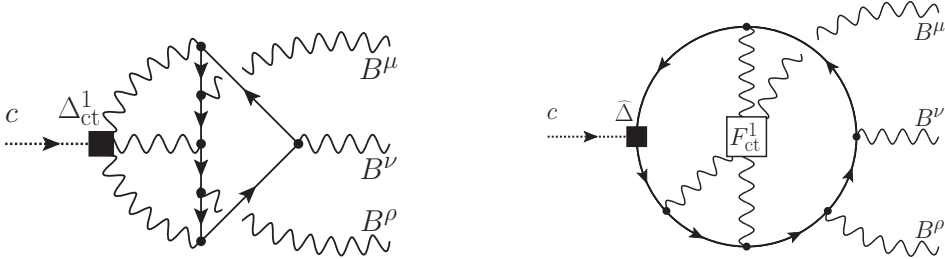


Figure 3: Representative 3-loop Feynman diagrams with counterterm insertions contributing to the 4-loop, subrenormalised, Δ -operator-inserted 1PI Green function $i\Delta \cdot \Gamma|_{B_\rho B_\nu B_\mu c}^4$. The left diagram features the insertion of a new Δ -vertex resulting from a 1-loop correction to the Δ -operator, while the right diagram involves the insertion of a 1-loop, finite, symmetry-restoring counterterm.

entative 3-loop counterterm diagrams that contribute to the 4-loop result for the Green function $cB^\mu B^\nu B^\rho$. The left diagram includes the insertion of a 1-loop correction to the Δ -operator, while the right diagram features the insertion of a 1-loop symmetry-restoring counterterm. Both of these counterterm vertices have no tree-level analogue, highlighting the increased structural complexity introduced by the required symmetry-restoration in the BMHV scheme.

Despite these challenges, the BMHV scheme remains viable for practical applications. This is primarily because the full renormalisation procedure needs to be performed only once. Once completed, physical observables can be computed just as in any other regularisation scheme, provided the BMHV algebra is consistently applied. Importantly, the

number of Green functions required for the calculation of a given observable does not increase, nor does the number of diagrams for the genuine L -loop contributions. Furthermore, Δ -vertices do no longer play a role in calculations of observables after the symmetry is restored. Only the number of counterterms is increased, yet even these remain manageable: as shown in Sec. 4, the resulting counterterms can be expressed in a compact form, even at the 4-loop level, making them well-suited for efficient computer implementations. Hence, the BMHV scheme is not only theoretically consistent, but also practically applicable for higher-order computations in chiral gauge theories.

3.3 BMHV Algebra with Non-Anticommuting γ_5

In the BMHV scheme, full anticommutativity of γ_5 is abandoned in D dimensions, which results in modified algebraic relations for the γ -matrices — the source of the regularisation-induced breaking of gauge and BRST invariance, see Eq. (2.9). In particular, the (quasi) D -dimensional space of DReg is decomposed into a 4- and a $(D - 4)$ -dimensional component as $\mathbb{M} = \mathbb{M}_4 \oplus \mathbb{M}_{D-4}$, see Refs. [20, 31, 33] and Ref. [6] for a review, where 4- and $(D - 4)$ -dimensional objects are denoted with overbars and hats, respectively. Thus, all Lorentz covariants admit a decomposition of the form

$$\gamma^\mu = \bar{\gamma}^\mu + \hat{\gamma}^\mu, \quad \eta_{\mu\nu} = \bar{\eta}_{\mu\nu} + \hat{\eta}_{\mu\nu}, \quad X^\mu = \bar{X}^\mu + \hat{X}^\mu, \quad (3.4)$$

for any Lorentz-vector X^μ and with

$$\bar{\eta}^{\mu\nu}\bar{\eta}_{\mu\nu} = 4, \quad \hat{\eta}^{\mu\nu}\hat{\eta}_{\mu\nu} = D - 4, \quad \bar{\eta}^{\mu\nu}\hat{\eta}_{\mu\nu} = 0. \quad (3.5)$$

This leads to the aforementioned modification of the γ -algebra

$$\begin{aligned} \{\bar{\gamma}^\mu, \bar{\gamma}^\nu\} &= 2\bar{\eta}^{\mu\nu}\mathbb{1}, & \{\hat{\gamma}^\mu, \hat{\gamma}^\nu\} &= 2\hat{\eta}^{\mu\nu}\mathbb{1}, & \{\bar{\gamma}^\mu, \hat{\gamma}^\nu\} &= 0, \\ \bar{\gamma}_\mu\bar{\gamma}^\mu &= 4\mathbb{1}, & \hat{\gamma}_\mu\hat{\gamma}^\mu &= (D - 4)\mathbb{1}, & \bar{\gamma}_\mu\hat{\gamma}^\mu &= 0, \end{aligned} \quad (3.6)$$

where γ_5 , as a manifestly 4-dimensional quantity, anticommutes only with the 4-dimensional components of the γ -matrices, $\bar{\gamma}^\mu$, and commutes with the evanescent components $\hat{\gamma}^\mu$, such that

$$\begin{aligned} \{\gamma_5, \bar{\gamma}^\mu\} &= 0, & [\gamma_5, \hat{\gamma}^\mu] &= 0, \\ [\gamma_5, \bar{\gamma}^\mu] &= 2\gamma_5\bar{\gamma}^\mu, & \{\gamma_5, \hat{\gamma}^\mu\} &= 2\gamma_5\hat{\gamma}^\mu. \end{aligned} \quad (3.7)$$

Further, the γ -traces are defined such that

$$\text{Tr}(\mathbb{1}) = 4, \quad \text{Tr}(\gamma^\mu) = 0. \quad (3.8)$$

In contrast to some other schemes, cyclicity of the trace is kept in D dimensions and

$$\text{Tr}(\gamma_5\bar{\gamma}^\mu\bar{\gamma}^\nu\bar{\gamma}^\rho\bar{\gamma}^\sigma) = -4i\varepsilon^{\mu\nu\rho\sigma} \quad (3.9)$$

is satisfied by the 4-dimensional part of the γ -matrices.

In FORM, we implemented these algebraic relations in such a way that terms cancel as soon as possible in order to increase computational performance at higher orders. For instance, this is done by making use of the fact that Lorentz index contractions between 4-dimensional and evanescent quantities vanish, e.g. $\bar{\eta}_{\mu\nu}\text{Tr}(\dots\hat{\gamma}^\nu\dots) = 0$.

Traces of γ -matrices require a focus on their own for our calculation. Although FORM is equipped with highly efficient built-in routines to deal with γ -traces, problems arise when

dealing with γ -matrices in D dimensions within the framework of the BMHV scheme. On the one hand D -dimensional traces in FORM cannot deal with γ_5 , and on the other hand the BMHV-algebra presented above is not implemented in FORM. We stress that traces of 4-dimensional γ -traces in FORM are optimised using dedicated rules and relations, such as the so-called Chisholm identity, in order to keep the number of generated terms small, see Ref. [38]. These algorithms are highly efficient, well-established and have thoroughly been tested over the past years. In order to make use of these optimisations as much as possible, we factorise every γ -trace into a D -dimensional part that does not contain γ_5 and a 4-dimensional part with possible occurrences of γ_5 .

First, each γ^μ -matrix is expressed via $\bar{\gamma}^\mu$ and $\hat{\gamma}^\mu$. In the case of D -dimensional matrices, this is either done via $\gamma^\mu = \bar{\gamma}^\mu + \hat{\gamma}^\mu$ or, slightly more efficient as it does not increase the number of terms, via

$$\text{Tr}(\dots \mathbb{P}_\alpha \gamma^\mu \mathbb{P}_\beta \dots) = \begin{cases} \text{Tr}(\dots \bar{\gamma}^\mu \mathbb{P}_R \dots), & \alpha = L, \beta = R, \\ \text{Tr}(\dots \bar{\gamma}^\mu \mathbb{P}_L \dots), & \alpha = R, \beta = L, \\ \text{Tr}(\dots \hat{\gamma}^\mu \mathbb{P}_R \dots), & \alpha = R, \beta = R, \\ \text{Tr}(\dots \hat{\gamma}^\mu \mathbb{P}_L \dots), & \alpha = L, \beta = L, \end{cases} \quad (3.10)$$

where $\mathbb{P}_{L/R} = (\mathbb{1} \mp \gamma_5)/2$, depending on the considered situation. Next, each γ -trace is brought into a “normal form”, where all evanescent matrices are on the left-most side inside the trace, while all 4-dimensional matrices are on the right-most side. This is achieved by applying the anticommutation relation $\bar{\gamma}^\mu \hat{\gamma}^\nu = -\hat{\gamma}^\nu \bar{\gamma}^\mu$, see Eq. (3.6). More specifically, this normal form takes the form

$$\text{Tr}(\hat{\gamma}^{\nu_1} \dots \hat{\gamma}^{\nu_m} \bar{\gamma}^{\mu_1} \dots \bar{\gamma}^{\mu_n} \mathbb{A}), \quad (3.11)$$

with $\mathbb{A} \in \{\mathbb{1}, \gamma_5, \mathbb{P}_L, \mathbb{P}_R\}$. Clearly, such traces are non-vanishing only if n and m are even integers. A trace of this form can then be factorised as

$$\text{Tr}(\hat{\gamma}^{\nu_1} \dots \hat{\gamma}^{\nu_m} \bar{\gamma}^{\mu_1} \dots \bar{\gamma}^{\mu_n} \mathbb{A}) = \frac{1}{4} \text{Tr}(\hat{\gamma}^{\nu_1} \dots \hat{\gamma}^{\nu_m}) \text{Tr}(\bar{\gamma}^{\mu_1} \dots \bar{\gamma}^{\mu_n} \mathbb{A}). \quad (3.12)$$

A concise proof of this formula is provided in App. A. In FORM, traces of the type $\text{Tr}(\hat{\gamma}^{\nu_1} \dots \hat{\gamma}^{\nu_m})$ can be evaluated with the built-in D -dimensional γ -trace algorithms, while traces of the type $\text{Tr}(\bar{\gamma}^{\mu_1} \dots \bar{\gamma}^{\mu_n} \mathbb{A})$ can be handled by the built-in 4-dimensional γ -trace algorithms utilising all algorithmic benefits. For the latter, the occurrence of γ_5 does not result in any problems as these traces are now handled in purely 4 dimensions. Clearly, the BMHV-algebra, as shown in Eqs. (3.5) to (3.7), must be implemented in FORM by hand and every step towards Eq. (3.12) must respect it.

3.4 Tadpole Decomposition

As mentioned above, in order to extract UV divergences, we employ a tadpole decomposition following the approach of Refs. [63, 64]. This method is based on recursively applying the exact identity

$$\frac{1}{(k+p)^2} = \frac{1}{k^2 - M^2} - \frac{p^2 + 2k \cdot p + M^2}{k^2 - M^2} \frac{1}{(k+p)^2} \quad (3.13)$$

to the propagators, where k denotes a loop momentum or any linear combination thereof, and M is an auxiliary mass scale. The expansion is performed to an order sufficient to capture all UV-divergent contributions.

While Eq. (3.13) is exact, its direct use in the context of the tadpole decomposition proves to be inconvenient in automated multi-loop computations. In particular, higher order applications face challenges related to a consistent momentum routing across genuine L -loop and associated ($< L$)-loop counterterm-inserted Feynman diagrams, due to subdivergences. To circumvent these difficulties, we employ an improved tadpole expansion, as suggested in Refs. [63, 64] and elaborated in detail in Ref. [65] (see also Ref. [33]). In this approach, the auxiliary mass parameter M is introduced uniformly in all propagators, and a Taylor-expansion in external momenta (and internal/physical masses, if present) is performed. The expansion is truncated at the order determined by the superficial degree of divergence of the considered Green function. For example, for a massless propagator $(k+p)^{-2}$, we obtain

$$\begin{aligned} \frac{1}{(k+p)^2 - M^2} &= \frac{1}{k^2 - M^2} - \frac{2k \cdot p}{(k^2 - M^2)^2} - \frac{p^2}{(k^2 - M^2)^2} + \frac{4(k \cdot p)^2}{(k^2 - M^2)^3} \\ &+ \frac{4p^2 k \cdot p}{(k^2 - M^2)^3} - \frac{8(k \cdot p)^3}{(k^2 - M^2)^4} + \mathcal{O}(p^4). \end{aligned} \quad (3.14)$$

Specifically, for the Green function cB^μ , which has degree of divergence 3 (see Fig. 1 for representative diagrams), the expansion must be carried out up to third order, as shown in Eq. (3.14). In contrast, for the Green function $cB^\mu B^\nu B^\rho$, whose degree of divergence is 1 (see Fig. 2 and 3 for representative diagrams), the expansion can be truncated after the second term on the RHS of Eq. (3.14). In the case of the Green function $B^\mu B^\nu B^\rho B^\sigma$, only the zeroth-order term — independent of external momenta — must be retained, as its degree of divergence is 0.

Rearranging the terms on the RHS of Eq. (3.14) yields

$$\frac{1}{k^2 - M^2} - \frac{p^2 + 2k \cdot p}{(k^2 - M^2)^2} + \frac{(p^2 + 2k \cdot p)^2}{(k^2 - M^2)^3} + \dots, \quad (3.15)$$

which resembles the recursive application of the exact tadpole decomposition in Eq. (3.13) up to terms $\propto M^2$ in the numerator. In the Taylor-expansion approach, omitting such numerator terms $\propto M^2$ necessitates a systematic compensation at each order, particularly at the multi-loop level in the presence of subdivergences. This is achieved by including all required auxiliary counterterms proportional to M^2 in order to subtract the effect of the missing numerator terms $\propto M^2$. Both the auxiliary mass parameter M^2 and the auxiliary mass counterterms are used only for technical purposes in the evaluation of the Feynman integrals, and are not intrinsic to the theory. In particular, the auxiliary mass counterterm associated to the gauge boson does not break gauge invariance, as it does not enter the action.

To some extent, this method addresses both issues outlined in Sec. 3.2 by decomposing all integrals into tadpoles without external momenta, thereby reducing the computational complexity in certain aspects. This allows the renormalisation of chiral gauge theories in the BMHV scheme at higher loop orders, where Green functions with up to five external legs must be computed. Its main drawback, however, is the proliferation of terms that arises after decomposing the integrand according to Eq. (3.14), particularly for Green functions with a high degree of divergence, such as cB^μ .

3.5 Practical Implementation of Counterterms

In practice, we implemented counterterm insertions into propagators in FORM by employing modified propagator expressions, which are applied recursively depending on the required insertion order. For fermions, we have

$$\mathcal{D}_{f,ij}(k) = \frac{ik}{k^2} \left(\delta_{ij} + i \sum_{\alpha,\beta \in \{L,R\}} \delta Z_{\bar{\alpha}\beta,ik}^f \mathbb{P}_\alpha \not{k} \mathbb{P}_\beta \mathcal{D}_{f,kj}(k) \right), \quad (3.16)$$

where an index with a bar, e.g. $\bar{\alpha}$, denotes the opposite chirality of the actual index, i.e. $\bar{\alpha} = R$ for $\alpha = L$. For the gauge boson, the propagator takes the form

$$\begin{aligned} \mathcal{D}_g^{\mu\nu}(k) = & \frac{-i}{k^2} \left(\eta^{\mu\rho} - (1-\xi) \frac{k^\mu k^\rho}{k^2} \right) \left(\delta_\rho^\nu - i \left[-\delta \bar{Z}_M^g M^2 \bar{\eta}_{\rho\sigma} - \delta \hat{Z}_M^g M^2 \hat{\eta}_{\rho\sigma} \right. \right. \\ & + \delta Z_D^g (\eta_{\rho\sigma} k^2 - k_\rho k_\sigma) + \delta \bar{Z}_{4D}^g (\bar{\eta}_{\rho\sigma} \bar{k}^2 - \bar{k}_\rho \bar{k}_\sigma) \\ & + \delta \bar{Z}_{11}^g \bar{\eta}_{\rho\sigma} \bar{k}^2 + \delta \hat{Z}_{12}^g \bar{\eta}_{\rho\sigma} \hat{k}^2 + \delta \hat{Z}_{21}^g \hat{\eta}_{\rho\sigma} \bar{k}^2 + \delta \hat{Z}_{22}^g \hat{\eta}_{\rho\sigma} \hat{k}^2 \\ & \left. \left. - \delta \bar{Z}_{33}^g \bar{k}_\rho \bar{k}_\sigma - \delta \hat{Z}_{34}^g \bar{k}_\rho \hat{k}_\sigma - \delta \hat{Z}_{43}^g \hat{k}_\rho \bar{k}_\sigma - \delta \hat{Z}_{44}^g \hat{k}_\rho \hat{k}_\sigma \right] \mathcal{D}_g^{\sigma\nu}(k) \right). \end{aligned} \quad (3.17)$$

This approach is similar to that of Ref. [59], but adapted to our calculation in the BMHV scheme. In particular, the counterterm contributions in the propagators include all possible Lorentz covariants. For each δZ , a perturbative expansion is implied.³ In the case of the gauge boson propagator, the first and the last two lines of Eq. (3.17) already form a complete basis. For convenience, we also include the second line, which introduces both D - and 4-dimensional transversal combinations that frequently appear in practical applications, albeit with some redundancy. In non-Abelian gauge theories with interacting ghosts or theories with scalar bosons, analogous propagators have to be implemented for the ghosts and the scalars, respectively.

Counterterm insertions for interaction vertices are implemented straightforwardly. For instance, the gauge interaction is given by

$$-ig \sum_{\alpha,\beta \in \{L,R\}} (\mathcal{Y}_{\bar{\alpha}\beta,ij} + \delta \mathcal{Y}_{\bar{\alpha}\beta,ij}) \mathbb{P}_\alpha \gamma^\mu \mathbb{P}_\beta. \quad (3.18)$$

This expression represents a general implementation that includes both left- and right-handed fermions, as well as evanescent gauge interactions.

In contrast to the theory discussed in Ref. [25], the right-handed model considered in this work, see Sec. 2, has only nonzero $\mathcal{Y}_{RR} \equiv \mathcal{Y}_R$, while all other hypercharge matrices vanish. Consequently, left-handed and evanescent gauge interactions are absent, which in turn reduces the number of required counterterms. Accordingly, from the subset of counterterms listed above, we specifically need δZ_{RR}^f , $\delta \bar{Z}_M^g$, $\delta \bar{Z}_{4D}^g$, $\delta \bar{Z}_{11}^g$, $\delta \hat{Z}_{12}^g$ and $\delta \mathcal{Y}_{RR}$. In Sec. 4 we will decompose these renormalisation constants further into symmetric contributions δZ , non-symmetric contributions with $1/\epsilon$ -poles δX , and finite symmetry-restoring counterterms \mathcal{F} . With this convention, the corresponding 4-loop renormalisation con-

³The δZ 's do not generally result from a multiplicative renormalisation transformation, as they also account for symmetry-restoring counterterms.

stants in the model of Sec. 2 take the form

$$\begin{aligned}
\delta Z_{RR,ij}^{f,(4)} &= \frac{g^8}{(16\pi^2)^4} \left(\delta Z_{\psi,ij}^{(4)} + \delta \bar{X}_{\psi\psi,ij}^{(4)} + \mathcal{F}_{\psi\psi,ij}^{4,\text{break}} \right), \\
\delta \bar{Z}_{4D}^{g,(4)} &= \frac{g^8}{(16\pi^2)^4} \delta Z_B^{(4)}, \\
\delta \bar{Z}_{11}^{g,(4)} &= \frac{g^8}{(16\pi^2)^4} \left(\delta \bar{X}_{BB}^{(4)} + \mathcal{F}_{BB}^{4,\text{break}} \right), \\
\delta \hat{Z}_{12}^{g,(4)} &= \frac{g^8}{(16\pi^2)^4} \delta \hat{X}_{BB}^{(4)}, \\
\delta \mathcal{Y}_{RR,ij}^{(4)} &= \frac{g^8}{(16\pi^2)^4} (\mathcal{Y}_R)_{ik} \delta Z_{\psi,kj}^{(4)},
\end{aligned} \tag{3.19}$$

with explicit expressions provided in Sec. 4. In addition, although not displayed explicitly here, symmetry-restoring quartic gauge boson counterterms $\delta \bar{Z}_{4g}$ and quantum corrections to the Δ -operator are also required for the full renormalisation procedure, as discussed in Sec. 4.

3.6 Tensor Reduction

Calculations in gauge theories lead to tensor integrals $I^{\mu_1 \dots \mu_r}$ of rank r , which we map to scalar integrals using tensor reduction. One starts by writing the tensor integral as a linear combination of all possible Lorentz tensors $T_a^{\mu_1 \dots \mu_r}$ allowed by symmetries:

$$I^{\mu_1 \dots \mu_r}(p_1, \dots, p_E) = \sum_{a=1}^n C_a(p_1, \dots, p_E) T_a^{\mu_1 \dots \mu_r}(p_1, \dots, p_E). \tag{3.20}$$

The tensors $T_a^{\mu_1 \dots \mu_r}$ are independent of the perturbative order and the coefficients C_a consist of scalar loop integrals.

After applying the tadpole decomposition, as discussed in Sec. 3.4, the resulting vacuum bubble tensor integrals do not depend on external momenta p_i . Thus, both the tensors $T_a^{\mu_1 \dots \mu_r}$ and the coefficients C_a are independent of external momenta. For this reason, the tensors $T_a^{\mu_1 \dots \mu_r}$ are solely composed of products of metric tensors $\eta^{\mu\nu}$. These metric tensors are D -dimensional, resulting in purely D -dimensional projectors, in line with the discussion in Sec. 3.2.

In this work, we employ the method proposed and applied in Refs. [58, 66] for an efficient tensor reduction of such vacuum bubble tensor integrals. During the course of this project, two other groups published work on tensor reduction, including external momenta and providing further mathematical insights, see Refs. [67] and [68]. Notably, the group of Ref. [68] provided a detailed discussion of the method employed here — naming it *orbit partition approach* — and published the tensor reduction software tool `OPITeR` [69]. Nonetheless, we find it valuable to document our implementation of this method for the reduction of vacuum bubble tensor integrals, specifically because all computations in this project have been performed using our own `FORM` programs.

In a nutshell, the tensor reduction consists of two main tasks. The first task is the construction of a basis \mathcal{B} of all tensor structures $T_a^{\mu_1 \dots \mu_r}$ contributing to a general tensor, see Eq. (3.20), and the determination of projectors $P_a^{\mu_1 \dots \mu_r}$ to calculate the coefficients

C_a . The projectors (dual tensors) are constructed from the basic tensors $T_a^{\mu_1 \dots \mu_r}$ as well and form the dual basis \mathcal{B}^* . They are required to satisfy the orthonormality relation

$$P_a^{\mu_1 \dots \mu_r} T_{b, \mu_1 \dots \mu_r} = \delta_{ab}. \quad (3.21)$$

This first task can be done once and in advance of the calculation of Green functions. We collect the resulting projectors in so-called tensor reduction tables. The second task is the application of the projectors to the specific tensor integrals of interest to obtain explicit expressions for the coefficients C_a . Condition (3.21) implies that the coefficients C_a are obtained upon projection via

$$C_a = P_a^{\mu_1 \dots \mu_r} I_{\mu_1 \dots \mu_r} \quad (3.22)$$

for a given loop integral $I_{\mu_1 \dots \mu_r}$.

Constructing the tensor reduction tables: In the present case of vacuum bubbles, only tensor integrals of even rank r give rise to non-vanishing contributions and, as mentioned above, the only possible Lorentz covariants are metric tensors $\eta^{\mu\nu}$. Hence, following Eq. (3.20), these vacuum bubble tensor integrals can be decomposed into a linear combination of $n = |S_2^r| = (r-1)!! = r!/(2^{r/2}(r/2)!)$ independent tensors

$$T_\sigma^{\mu_1 \dots \mu_r} = \eta^{\mu_{\sigma(1)} \mu_{\sigma(2)}} \dots \eta^{\mu_{\sigma(r-1)} \mu_{\sigma(r)}}, \quad (3.23)$$

composed of $r/2$ metric tensors each. S_2^r is the set of permutations that generate all distinct products of metric tensors of rank r , i.e. all $T_a^{\mu_1 \dots \mu_r}$.

Clearly, the projectors can only consist of such products of metric tensors as well. Therefore, with all possible tensor structures $T_a^{\mu_1 \dots \mu_r}$ at hand, the projectors are generally given as a linear combination of these tensor structures as

$$P_a^{\mu_1 \dots \mu_r} = \sum_{b=1}^n A_b^{(a)} T_b^{\mu_1 \dots \mu_r}, \quad (3.24)$$

with yet unknown coefficients $A_b^{(a)}$.

Using the orthonormality relation (3.21) for a fixed $a \in \{1, \dots, n\}$, we obtain n equations for n coefficients $A_b^{(a)}$ upon contraction with the n tensors $\{T_b^{\mu_1 \dots \mu_r}\}_{b=1}^n = \mathcal{B}$. Solving this system of equations determines the projector $P_a^{\mu_1 \dots \mu_r}$. Indeed, in this way all projectors $P_a^{\mu_1 \dots \mu_r}$, $\forall a \in \{1, \dots, n\}$, are determined, since all other projectors (with $b \neq a$) can be obtained by permutations of Lorentz indices.⁴ However, solving this system of equations means inverting an $n \times n$ matrix. This becomes a major challenge as n is growing very fast with the tensor rank r , see Tab. 2.

This problem can be approached using symmetry arguments, as explained in Refs. [58, 66–68], which effectively reduce the size of the system of equations significantly. In particular, for a rank r tensor integral, the projector $P_a^{\mu_1 \dots \mu_r}$ is invariant under the same (index permutation) symmetries as the tensor $T_a^{\mu_1 \dots \mu_r}$, given by the corresponding *stabiliser subgroup* $H(T_a)$. For fixed $a \in \{1, \dots, n\}$, all tensors $\{T_b^{\mu_1 \dots \mu_r}\}_{b=1}^n$ can be grouped into m disjoint *orbits* $\{\Theta_c^{(a)}\}_{c=1}^m$, each consisting of tensors that transform into

⁴Given $\sigma \in S_r$, such that $\sigma \circ T_a^{\mu_1 \dots \mu_r} = T_b^{\mu_1 \dots \mu_r}$, then $P_b^{\mu_1 \dots \mu_r} = \sigma \circ P_a^{\mu_1 \dots \mu_r}$.

r	2	4	6	8	10	12	14	16
$n = S_2^r $	1	3	15	105	945	10395	135135	2027025
$m = p(r/2)$	1	2	3	5	7	11	15	22

Table 2: Numbers n and m of independent tensor structures of rank r vacuum tensor integrals and integer partitions of $r/2$, respectively, for $r \leq 16$.

one another under the action of $H(T_a)$, forming a partition of \mathcal{B} . For each $c \in \{1, \dots, m\}$, the sum of all elements of ${}_r\Theta_c^{(a)}$ resembles a tensor that has the same (permutation) symmetries as $T_a^{\mu_1 \dots \mu_r}$, i.e. is invariant under $H(T_a)$. Due to these symmetry properties, all tensors of a given orbit come with the same coefficient $A_c^{(a)}$. Thus, the RHS of Eq. (3.24) can be rearranged to

$$P_a^{\mu_1 \dots \mu_r} = \sum_{c=1}^m A_c^{(a)} \left(\sum_{T \in {}_r\Theta_c^{(a)}} T^{\mu_1 \dots \mu_r} \right), \quad (3.25)$$

with m coefficients $A_c^{(a)}$. Since each bracketed sum of tensors on the RHS of Eq. (3.25) is stabilised under $H(T_a)$ by construction, this Ansatz automatically ensures the correct symmetry properties.

The number of orbits m depends on the rank r of the problem and is determined by the number of the possible index-contraction *cycles*. These *cycles* are closed contraction loops formed between the Lorentz indices of the metric tensors in $T_a^{\mu_1 \dots \mu_r}$ and those in a considered tensor $T_{b, \mu_1 \dots \mu_r}$. For fixed a , tensors $T_{b, \mu_1 \dots \mu_r}$ that belong to the same orbit ${}_r\Theta_c^{(a)}$ can thus be identified by the respective number of cycles. The number of maximally possible cycles is equal to the number of integer partitions of $r/2$, and hence m grows significantly slower than n , as shown in Tab. 2. Consequently, for fixed $a \in \{1, \dots, n\}$, contracting the projector $P_a^{\mu_1 \dots \mu_r}$ with a single representative tensor from each of the m orbits ${}_r\Theta_c^{(a)}$ and using the orthonormality relation (3.21) results in only m equations for m coefficients $A_c^{(a)}$. Solving this system of equations constitutes a significant simplification compared to the original one of n equations, cf. Tab. 2. We label the orbits $\{{}_r\Theta_c^{(a)}\}_{c=1}^m$ such that the orbit with $c = 1$ contains the tensors exhibiting the maximal number of index-contraction cycles with $T_a^{\mu_1 \dots \mu_r}$, and the $c = m$ orbit those with the minimal number, i.e. a single cycle. Notably, the orbit with $c = 1$ consists of only one tensor, the tensor $T_a^{\mu_1 \dots \mu_r}$ itself. The construction of these orbits via contraction cycles is best illustrated with an explicit example.

In the following, let us consider a tensor integral problem of rank $r = 6$: After identifying all $n = 15$ independent tensors, $\mathcal{B} = \{\sigma \circ T^{\mu_1 \dots \mu_6} \mid \sigma \in S_2^6\}$, cf. Eq. (3.23), we can, w.l.o.g., focus on fixed $a = 1$ and construct $P_1^{\mu_1 \dots \mu_6}$ according to Eq. (3.25). To achieve this, we analyse the Lorentz index contractions of

$$T_1^{\mu_1 \dots \mu_6} = \eta^{\mu_1 \mu_2} \eta^{\mu_3 \mu_4} \eta^{\mu_5 \mu_6} \quad (3.26)$$

with $\{T_{b, \mu_1 \dots \mu_6}\}_{b=1}^{15}$ in order to identify all orbits $\{{}_6\Theta_c^{(1)}\}_{c=1}^m$ (with yet unknown m). Indeed, in the present case of $r = 6$, we can identify a maximum of $m = 3$ disjoint cycles of index contractions, which is exactly the number of integer partitions of $r/2$. As mentioned above, the first orbit ${}_6\Theta_1^{(1)}$ consists solely of $T_{1, \mu_1 \dots \mu_6}$, since it is the only tensor that can

be reached by acting with $h \in H(T_1)$ on itself, and thus inherently possesses already on its own the same permutation symmetry as $T_1^{\mu_1 \dots \mu_6}$. Moreover, because of this, it can be identified as the only tensor which admits the most possible contraction cycles with $T_1^{\mu_1 \dots \mu_6}$, provided by

$$\eta^{\mu_1 \mu_2} \eta^{\mu_3 \mu_4} \eta^{\mu_5 \mu_6} \eta_{\mu_1 \mu_2} \eta_{\mu_3 \mu_4} \eta_{\mu_5 \mu_6}. \quad (3.27)$$

In particular, these cycles are given by $1 \rightarrow 2 \rightarrow 1$, $3 \rightarrow 4 \rightarrow 3$ and $5 \rightarrow 6 \rightarrow 5$, fixing $m = 3$ in the case of $r = 6$. Hence, for the first orbit, we find

$${}_6\Theta_1^{(1)} \equiv \{T_{1, \mu_1 \dots \mu_6} = \eta_{\mu_1 \mu_2} \eta_{\mu_3 \mu_4} \eta_{\mu_5 \mu_6}\}. \quad (3.28)$$

Next, the second orbit, ${}_6\Theta_2^{(1)}$, is filled with all tensors that admit two contraction cycles with $T_1^{\mu_1 \dots \mu_6}$. For instance, this is the case for the tensor $T_{4, \mu_1 \dots \mu_6} = \eta_{\mu_1 \mu_3} \eta_{\mu_2 \mu_4} \eta_{\mu_5 \mu_6}$, where we find

$$\eta^{\mu_1 \mu_2} \eta^{\mu_3 \mu_4} \eta^{\mu_5 \mu_6} \eta_{\mu_1 \mu_3} \eta_{\mu_2 \mu_4} \eta_{\mu_5 \mu_6}, \quad (3.29)$$

i.e. the two cycles $1 \rightarrow 3 \rightarrow 4 \rightarrow 2 \rightarrow 1$ and $5 \rightarrow 6 \rightarrow 5$, and analogously for all other $T_{b, \mu_1 \dots \mu_6} \in {}_6\Theta_2^{(1)}$. Thus, we have

$${}_6\Theta_2^{(1)} \equiv \{\eta_{\mu_1 \mu_2} \eta_{\mu_3 \mu_5} \eta_{\mu_4 \mu_6}, \eta_{\mu_1 \mu_2} \eta_{\mu_3 \mu_6} \eta_{\mu_4 \mu_5}, \eta_{\mu_1 \mu_3} \eta_{\mu_2 \mu_4} \eta_{\mu_5 \mu_6}, \eta_{\mu_1 \mu_4} \eta_{\mu_2 \mu_3} \eta_{\mu_5 \mu_6}, \eta_{\mu_1 \mu_5} \eta_{\mu_2 \mu_6} \eta_{\mu_3 \mu_4}, \eta_{\mu_1 \mu_6} \eta_{\mu_2 \mu_5} \eta_{\mu_3 \mu_4}\}. \quad (3.30)$$

Finally, the last orbit ${}_6\Theta_3^{(1)}$ is given by all tensors that have only one index-contraction cycle with $T_1^{\mu_1 \dots \mu_6}$. An example for this set is provided by $T_{10, \mu_1 \dots \mu_6} = \eta_{\mu_1 \mu_5} \eta_{\mu_2 \mu_3} \eta_{\mu_4 \mu_6}$. In this case, we find

$$\eta^{\mu_1 \mu_2} \eta^{\mu_3 \mu_4} \eta^{\mu_5 \mu_6} \eta_{\mu_1 \mu_5} \eta_{\mu_2 \mu_3} \eta_{\mu_4 \mu_6}, \quad (3.31)$$

indeed, with only one cycle $1 \rightarrow 5 \rightarrow 6 \rightarrow 4 \rightarrow 3 \rightarrow 2 \rightarrow 1$. Hence, the last orbit is found to be

$${}_6\Theta_3^{(1)} \equiv \{\eta_{\mu_1 \mu_3} \eta_{\mu_2 \mu_5} \eta_{\mu_4 \mu_6}, \eta_{\mu_1 \mu_3} \eta_{\mu_2 \mu_6} \eta_{\mu_4 \mu_5}, \eta_{\mu_1 \mu_4} \eta_{\mu_2 \mu_5} \eta_{\mu_3 \mu_6}, \eta_{\mu_1 \mu_4} \eta_{\mu_2 \mu_6} \eta_{\mu_3 \mu_5}, \eta_{\mu_1 \mu_5} \eta_{\mu_2 \mu_3} \eta_{\mu_4 \mu_6}, \eta_{\mu_1 \mu_5} \eta_{\mu_2 \mu_4} \eta_{\mu_3 \mu_6}, \eta_{\mu_1 \mu_6} \eta_{\mu_2 \mu_3} \eta_{\mu_4 \mu_5}, \eta_{\mu_1 \mu_6} \eta_{\mu_2 \mu_4} \eta_{\mu_3 \mu_5}\}. \quad (3.32)$$

Therefore, the projector $P_1^{\mu_1 \dots \mu_6}$ is given according to Eq. (3.25) with $m = 3$ different coefficients $\{A_c^{(1)}\}_{c=1}^3$ and tensors provided in the orbits (3.28), (3.30) and (3.32). Contracting the projector $P_1^{\mu_1 \dots \mu_6}$ with a representative tensor of each orbit in Eqs. (3.28), (3.30) and (3.32),⁵ and using the orthonormality relation (3.21), gives rise to the 3 equations

$$\begin{aligned} 1 &= P_1^{\mu_1 \dots \mu_6} T_{1, \mu_1 \dots \mu_6} = D^3 A_1^{(1)} + 6D^2 A_2^{(1)} + 8DA_3^{(1)}, \\ 0 &= P_1^{\mu_1 \dots \mu_6} T_{4, \mu_1 \dots \mu_6} = D^2 A_1^{(1)} + D(D^2 + D + 4)A_2^{(1)} + 4D(D + 1)A_3^{(1)}, \\ 0 &= P_1^{\mu_1 \dots \mu_6} T_{10, \mu_1 \dots \mu_6} = DA_1^{(1)} + 3D(D + 1)A_2^{(1)} + D(D^2 + 3D + 4)A_3^{(1)}. \end{aligned} \quad (3.33)$$

⁵Here, we used the same tensors as in the demonstrations in Eqs. (3.27), (3.29) and (3.31), i.e. $T_1^{\mu_1 \dots \mu_6}$, $T_4^{\mu_1 \dots \mu_6}$ and $T_{10}^{\mu_1 \dots \mu_6}$, respectively.

These equations lead to the three coefficients

$$\begin{aligned} A_1^{(1)} &= \frac{D^2 + 3D - 2}{(D^2 + 2D - 8)(D^2 + D - 2)D}, \\ A_2^{(1)} &= -\frac{1}{(D^2 + 2D - 8)(D - 1)D}, \\ A_3^{(1)} &= \frac{2}{(D^2 + 2D - 8)(D^2 + D - 2)D}, \end{aligned} \quad (3.34)$$

which determine the projector $P_1^{\mu_1 \dots \mu_6}$. All other projectors $P_{b \neq 1}^{\mu_1 \dots \mu_6}$ are then obtained by permutation of the Lorentz indices. In FORM, this is implemented via so-called wildcards.

Following this approach for all other tensor ranks, we have precomputed all coefficients and projectors up to tensor rank $r \leq 16$. These are written into tables and called during the execution of the tensor reduction routine in the FORM program.

Applying the tensor reduction to the tensor integrals: In contrast to the tensor reduction tables, which can be precomputed once, this task needs to be done for each tensor integral during the actual computation. It mainly amounts to determining the coefficients C_a associated to the considered tensor integral, see Eq. (3.22). Symmetry arguments can be used to optimise the performance of this task as well. In particular, the symmetry of the respective integrand of the tensor integral is used, which needs to remain unchanged upon tensor reduction.

In alignment with the example discussed above, we consider a rank $r = 6$ tensor integral of the form

$$I^{\mu_1 \dots \mu_6} = (\mu^{4-D})^L \int \left(\prod_{i=1}^L \frac{d^D k_i}{(2\pi)^D} \right) \frac{k_1^{\mu_1} k_1^{\mu_2} k_2^{\mu_3} k_2^{\mu_4} k_2^{\mu_5} k_2^{\mu_6}}{\mathcal{D}_1^{\nu_1} \dots \mathcal{D}_N^{\nu_N}} \quad (3.35)$$

to exemplarily illustrate the procedure. Clearly, the integrand of Eq. (3.35) admits an index permutation symmetry of the two Lorentz indices $\{\mu_1, \mu_2\}$ and the four Lorentz indices $\{\mu_3, \mu_4, \mu_5, \mu_6\}$ among each other, respectively. Due to this symmetry, the tensor integral decomposition, see Eq. (3.20), reduces to

$$I^{\mu_1 \dots \mu_6} = C_1 (T_1 + T_2 + T_3)^{\mu_1 \dots \mu_6} + C_4 (T_4 + T_5 + T_6 + \dots + T_{15})^{\mu_1 \dots \mu_6}, \quad (3.36)$$

with only two (instead of $n = 15$) distinct coefficients, such that each of the two summands is invariant under the same (index permutation) symmetry as the integrand in Eq. (3.35). The two coefficients can be obtained upon projection, see Eq. (3.22), as⁶

$$\begin{aligned} C_1 &= P_1^{\mu_1 \dots \mu_6} I_{\mu_1 \dots \mu_6} = \int \left(\prod_{i=1}^L \frac{d^D k_i}{(2\pi)^D} \right) \frac{(\mu^{4-D})^L}{\mathcal{D}_1^{\nu_1} \dots \mathcal{D}_N^{\nu_N}} \frac{(D+3)k_1^2 k_2^4 - 4(k_1 \cdot k_2)^2 k_2^2}{(D-1)D(D+2)(D+4)}, \\ C_4 &= P_4^{\mu_1 \dots \mu_6} I_{\mu_1 \dots \mu_6} = \int \left(\prod_{i=1}^L \frac{d^D k_i}{(2\pi)^D} \right) \frac{(\mu^{4-D})^L}{\mathcal{D}_1^{\nu_1} \dots \mathcal{D}_N^{\nu_N}} \frac{-k_1^2 k_2^4 + D(k_1 \cdot k_2)^2 k_2^2}{(D-1)D(D+2)(D+4)}. \end{aligned} \quad (3.37)$$

Hence, it is sufficient to contract the tensor integral with only one representative projector $P_a^{\mu_1 \dots \mu_6}$ for each coefficient C_a , where $P_a^{\mu_1 \dots \mu_6}$ admits the same index permutation

⁶Using the results for $A_c^{(1)}$ in Eq. (3.34).

symmetry as the respective term associated to the coefficient C_a . Utilising the symmetries of the integrand consequently reduces the computational effort needed to extract the required scalar integrals.

In FORM, we implemented this procedure via the built-in functions `dd_` and `distrib_`, in order to identify the different tensors that build the terms invariant under the integrand's symmetry, e.g. the two on the RHS of Eq. (3.36) associated to C_1 and C_4 , and to avoid generating duplicate terms by exploiting symmetries, as suggested in Ref. [66].

4 Four-Loop Renormalisation

Using the computational methods described in Sec. 3, we calculate all relevant subrenormalised Green functions and present the results for the complete 4-loop renormalisation of the chiral gauge theory discussed in the previous section. As outlined, the theory is regularised within the framework of the BMHV scheme of DReg, leading to a spurious breaking of gauge and BRST invariance. We construct the full 4-loop counterterm action, including the finite symmetry-restoring part, which renders the renormalised theory both finite and symmetric at this order. All 4-loop contributions have been computed in Feynman gauge, i.e. $\xi = 1$, and the anomaly cancellation condition, Eq. (2.4), has been imposed throughout. For a complete list of counterterms at the 1-, 2- and 3-loop level, we refer the reader to Refs. [31, 33].

The counterterm action S_{ct} admits a decomposition into a divergent part, S_{sct} , and a finite, symmetry-restoring part, S_{fct} . The divergent piece itself can further be split into a symmetric part, $S_{\text{sct,inv}}$, and a BRST-breaking part, $S_{\text{sct,break}}$. Hence, one obtains

$$S_{\text{ct}} = S_{\text{sct}} + S_{\text{fct}} = S_{\text{sct,inv}} + S_{\text{sct,break}} + S_{\text{fct}}. \quad (4.1)$$

This counterterm action S_{ct} , as well as its individual components $S_{\text{sct,inv}}$, $S_{\text{sct,break}}$ and S_{fct} , admits a perturbative expansion of the form

$$S_{\text{ct}} = S_{\text{ct}}^1 + S_{\text{ct}}^2 + S_{\text{ct}}^3 + S_{\text{ct}}^4 + \mathcal{O}(5\text{-loop}). \quad (4.2)$$

In Sec. 4.1, we provide the 4-loop results for the complete singular counterterm action, derived from the power-counting divergent 1PI Green functions listed below. These counterterms ensure UV finiteness of the theory at the 4-loop order.

Next, in Sec. 4.2, we discuss the 4-loop breaking of BRST symmetry. For this purpose, we concisely illustrate our methodology for symmetry restoration, based on quantum action principle of DReg, as explained in Refs. [20, 25, 31, 33, 35] (see Ref. [6] for a review). In particular, we extract the BRST-breaking contributions from 1PI Green functions with an insertion of a local Δ -operator, and provide explicit results for all relevant Green functions.

Using these results, we ultimately derive the complete set of finite, symmetry-restoring 4-loop counterterms in Sec. 4.3. Combined with the BRST-breaking part of the singular counterterm action, these counterterms restore the broken BRST symmetry, such that the renormalised theory satisfies the Slavnov-Taylor identity at the given order.

As outlined in Sec. 3.1, we thoroughly tested our setup in various ways. Moreover, the UV-divergent BRST-breaking contributions serve as a strong consistency check of our results, as they are obtained from both the standard 1PI Green functions provided

in Sec. 4.1 and Δ -inserted 1PI Green functions shown in Sec. 4.2. We find perfect agreement between both calculations. Additionally, all counterterms are local polynomials in external momenta, as they have to be as a matter of principle, which constitutes a further non-trivial cross-check and provides confidence in our results.

4.1 Four-Loop Singular Counterterm Action

We begin by providing all power-counting divergent, standard 1PI Green functions required to determine the singular counterterms. In the Abelian chiral gauge theory considered here, see Sec. 2, we obtain

$$i\Gamma_{B_\nu(-p)B_\mu(p)}|_{\text{div}}^4 = -\frac{ig^8}{(16\pi^2)^4} \delta Z_B^{(4)} \left(\bar{p}^\mu \bar{p}^\nu - \bar{p}^2 \bar{\eta}^{\mu\nu} \right) + \frac{ig^8}{(16\pi^2)^4} \left(\delta \widehat{X}_{BB}^{(4)} \bar{p}^2 \bar{\eta}^{\mu\nu} + \delta \overline{X}_{BB}^{(4)} \bar{p}^2 \bar{\eta}^{\mu\nu} \right), \quad (4.3)$$

$$i\Gamma_{\psi_j(p)\bar{\psi}_i(-p)}|_{\text{div}}^4 = -\frac{ig^8}{(16\pi^2)^4} \left(\delta Z_{\psi,ij}^{(4)} + \delta \overline{X}_{\bar{\psi},ij}^{(4)} \right) \bar{p} \mathbb{P}_R, \quad (4.4)$$

$$i\Gamma_{\psi_j(p_2)\bar{\psi}_i(p_1)B_\mu(q)}|_{\text{div}}^4 = \frac{ig^9}{(16\pi^2)^4} (\mathcal{Y}_R)_{ik} \delta Z_{\psi,kj}^{(4)} \bar{\gamma}^\mu \mathbb{P}_R, \quad (4.5)$$

$$i\Gamma_{B_\mu(q)B_\nu(p_1)B_\rho(p_2)}|_{\text{div}}^4 = 0, \quad (4.6)$$

$$i\Gamma_{B_\mu(p_2)B_\nu(p_1)B_\rho(p_4)B_\sigma(p_3)}|_{\text{div}}^4 = -\frac{ig^{10}}{(16\pi^2)^4} \delta \overline{X}_{BBBB}^{(4)} \left(\bar{\eta}^{\mu\nu} \bar{\eta}^{\rho\sigma} + \bar{\eta}^{\mu\rho} \bar{\eta}^{\nu\sigma} + \bar{\eta}^{\mu\sigma} \bar{\eta}^{\nu\rho} \right), \quad (4.7)$$

where Γ is the effective quantum action and all results are expressed in terms of counterterm coefficients. In particular, for the BRST-invariant contributions their Laurent expansions in ϵ are given by

$$\delta Z_B^{(4)} = \mathcal{A}_{BB}^{4,\text{inv}} \frac{1}{\epsilon} + \mathcal{B}_{BB}^{4,\text{inv}} \frac{1}{\epsilon^2} + \mathcal{C}_{BB}^{4,\text{inv}} \frac{1}{\epsilon^3}, \quad (4.8)$$

$$\delta Z_{\psi,ij}^{(4)} = \mathcal{A}_{\psi\psi,ij}^{4,\text{inv}} \frac{1}{\epsilon} + \mathcal{B}_{\psi\psi,ij}^{4,\text{inv}} \frac{1}{\epsilon^2} + \mathcal{C}_{\psi\psi,ij}^{4,\text{inv}} \frac{1}{\epsilon^3} + \mathcal{D}_{\psi\psi,ij}^{4,\text{inv}} \frac{1}{\epsilon^4}, \quad (4.9)$$

while for the BRST-breaking contributions we define

$$\delta \widehat{X}_{BB}^{(4)} = \widehat{\mathcal{A}}_{BB}^{4,\text{break}} \frac{1}{\epsilon} + \widehat{\mathcal{B}}_{BB}^{4,\text{break}} \frac{1}{\epsilon^2} + \widehat{\mathcal{C}}_{BB}^{4,\text{break}} \frac{1}{\epsilon^3} + \widehat{\mathcal{D}}_{BB}^{4,\text{break}} \frac{1}{\epsilon^4}, \quad (4.10)$$

$$\delta \overline{X}_{BB}^{(4)} = \overline{\mathcal{A}}_{BB}^{4,\text{break}} \frac{1}{\epsilon} + \overline{\mathcal{B}}_{BB}^{4,\text{break}} \frac{1}{\epsilon^2}, \quad (4.11)$$

$$\delta \overline{X}_{BBBB}^{(4)} = \overline{\mathcal{A}}_{BBBB}^{4,\text{break}} \frac{1}{\epsilon} + \overline{\mathcal{B}}_{BBBB}^{4,\text{break}} \frac{1}{\epsilon^2}, \quad (4.12)$$

$$\delta \overline{X}_{\bar{\psi},ij}^{(4)} = \overline{\mathcal{A}}_{\bar{\psi},ij}^{4,\text{break}} \frac{1}{\epsilon} + \overline{\mathcal{B}}_{\bar{\psi},ij}^{4,\text{break}} \frac{1}{\epsilon^2} + \overline{\mathcal{C}}_{\bar{\psi},ij}^{4,\text{break}} \frac{1}{\epsilon^3}. \quad (4.13)$$

We obtained analytical results for all of these pole coefficients in terms of the hypercharge matrix and Riemann zeta values. The explicit expressions are somewhat lengthy and therefore provided in App. B.

From these 1PI Green functions, we can now derive the complete singular counterterm action. On the one side, the BRST-invariant part takes the form

$$S_{\text{sct,inv}}^4 = \frac{g^8}{(16\pi^2)^4} \int d^D x \left\{ \delta Z_B^{(4)} \left(-\frac{1}{4} \overline{F}^{\mu\nu} \overline{F}_{\mu\nu} \right) + \delta Z_{\psi,kj}^{(4)} \bar{\psi}_i i \overline{\mathcal{D}}_{R,ik} \psi_j \right\}, \quad (4.14)$$

with right-handed covariant derivative

$$\bar{D}_{R,ij}^\mu = \left(\bar{\partial}^\mu \delta_{ij} + ig\mathcal{Y}_{R,ij} \bar{B}^\mu \right) \mathbb{P}_R. \quad (4.15)$$

On the other side, the BRST-breaking part of the singular counterterm action reads

$$S_{\text{sct,break}}^4 = \frac{g^8}{(16\pi^2)^4} \int d^D x \left\{ \delta \hat{X}_{BB}^{(4)} \frac{1}{2} \bar{B}_\mu \hat{\partial}^2 \bar{B}^\mu + \delta \bar{X}_{BB}^{(4)} \frac{1}{2} \bar{B}_\mu \bar{\partial}^2 \bar{B}^\mu \right. \\ \left. + g^2 \delta \bar{X}_{BBBB}^{(4)} \frac{1}{8} \bar{B}_\mu \bar{B}^\mu \bar{B}_\nu \bar{B}^\nu + \delta \bar{X}_{\bar{\psi}\psi,ij}^{(4)} \left(\bar{\psi}_i i \bar{\not{D}} \mathbb{P}_R \psi_j \right) \right\}. \quad (4.16)$$

It is straightforward to see that Eq. (4.14) is BRST-invariant, given the structure of the field monomials. Further, $S_{\text{sct,inv}}^4$ retains the same structure as at lower orders, see Refs. [31, 33]. In fact, its principal structure is the same as in ordinary vector-like QED, differing only in the use of a right-handed covariant derivative and modified coefficients. This is because it consists only of symmetric field combinations present in the tree-level Lagrangian and corresponds to a multiplicative field and parameter renormalisation of the gauge boson and the fermion fields, as well as the gauge coupling, such that the product gB^μ does not renormalise, just as in ordinary QED.

The BRST-breaking part of the counterterm action, given in Eq. (4.16), does also not introduce any new field monomials compared to the 3-loop case, cf. Ref. [33]. This contrasts with the transitions from 1 to 2 loops and from 2 to 3 loops, where new field monomials emerged at the higher loop order. Hence, the principal structure of the 4-loop BRST-breaking singular counterterm action remains the same as at the 3-loop order, with the only difference being the presence of higher order ϵ -poles in the counterterm coefficients. The absence of new field monomials is due to constraints imposed by power-counting and renormalisability, as well as the absence of evanescent gauge and Yukawa interactions, see also Ref. [25].

In analogy to the discussion in Ref. [33], we choose to attribute the BRST breaking entirely to the bilinear fermion terms, see Eq. (4.16). However, in the present context, this is just a choice and we also could have chosen the fermion-gauge boson vertex correction to carry the BRST breaking (or distribute it between both) using a slight rearrangement. In particular, we could rewrite these terms as

$$\frac{g^8}{(16\pi^2)^4} \int d^D x \left\{ \left(\delta Z_{\psi,kj}^{(4)} + \delta \bar{X}_{\bar{\psi}\psi,kj}^{(4)} \right) \bar{\psi}_i i \bar{\not{D}}_{R,ik} \psi_j + g \mathcal{Y}_{R,ik} \delta \bar{X}_{\bar{\psi}\psi,kj}^{(4)} \bar{\psi}_i \bar{\not{B}} \mathbb{P}_R \psi_j \right\}, \quad (4.17)$$

which leads to the same counterterm action, S_{sct}^4 , but with the BRST breaking fully attributed to the gauge interaction. We emphasise that this freedom depends on the specific model under consideration, as will be discussed in more detail at the end of Sec. 4.3.

4.2 Four-Loop BRST Breaking

Ultimately, we require the renormalised theory in 4 dimensions to satisfy the Slavnov-Taylor identity, i.e.

$$\text{LIM}_{D \rightarrow 4} (\mathcal{S}_D(\Gamma_{\text{DRen}})) = 0, \quad (4.18)$$

where \mathcal{S}_D is the D -dimensional Slavnov-Taylor operator, Γ_{DRen} denotes the renormalised effective quantum action in D dimensions and $\text{LIM}_{D \rightarrow 4}$ includes the limit $D \rightarrow 4$ and

dropping finite evanescent terms, i.e. evanescent Lorentz structures whose coefficients contain no poles in ϵ . The symmetry-restoring counterterms must be adjusted such that Eq. (4.18) becomes valid and thus the breaking induced by the BMHV regularisation is cancelled. As the crucial preliminary step, the breaking of Eq. (4.18) on the regularised level has to be evaluated. Following Refs. [6, 20, 25, 31, 33, 35], an efficient way to obtain this breaking is to utilise the quantum action principle of DReg, see Refs. [2–4] and Ref. [6] for a review, and rewrite the symmetry-breaking as an insertion of a local composite operator as

$$\mathcal{S}_D(\Gamma_{\text{DReg}}) = \Delta \cdot \Gamma_{\text{DReg}}. \quad (4.19)$$

The Δ -operator on the RHS of Eq. (4.19) is defined by

$$\Delta = \widehat{\Delta} + \Delta_{\text{ct}} = \mathcal{S}_D(S_0 + S_{\text{ct}}). \quad (4.20)$$

For practical perturbative calculations, we plug Eq. (4.19) into Eq. (4.18) and obtain the perturbative requirement

$$\text{LIM}_{D \rightarrow 4} \left(\widehat{\Delta} \cdot \Gamma_{\text{DReg}}^L + \sum_{k=1}^{L-1} \Delta_{\text{ct}}^k \cdot \Gamma_{\text{DReg}}^{L-k} + \Delta_{\text{ct}}^L \right) = 0, \quad \forall L \geq 1, \quad (4.21)$$

where L is the loop order of the respective quantities and the local composite operator Δ admits the following perturbative expansion:

$$\Delta = \widehat{\Delta} + \Delta_{\text{ct}}^1 + \Delta_{\text{ct}}^2 + \Delta_{\text{ct}}^3 + \Delta_{\text{ct}}^4 + \mathcal{O}(5\text{-loop}). \quad (4.22)$$

While $\widehat{\Delta}$ represents the breaking of BRST symmetry at tree-level, the operator Δ_{ct}^L reflects the breaking at loop order L . Hence, using Eq. (4.21) as a starting point, we can compute the 4-loop BRST breaking Δ_{ct}^4 from⁷

$$(\Delta \cdot \Gamma)^4 = \widehat{\Delta} \cdot \Gamma^4 + \Delta_{\text{ct}}^1 \cdot \Gamma^3 + \Delta_{\text{ct}}^2 \cdot \Gamma^2 + \Delta_{\text{ct}}^3 \cdot \Gamma^1 = -\Delta_{\text{ct}}^4 + \mathcal{O}(\cdot), \quad (4.23)$$

where $\mathcal{O}(\cdot)$ indicates finite evanescent terms that ultimately drop out in the limit $\text{LIM}_{D \rightarrow 4}$ in Eq. (4.18). Notably, to obtain the complete result for the BRST breaking, including both divergent and finite contributions, we can restrict ourselves to power-counting divergent, subnormalised 1PI Green functions with an insertion of the Δ -operator. The reason for this is that the lowest-order part of the Δ -operator, i.e. $\widehat{\Delta}$ arising from the tree-level breaking of BRST invariance, is purely evanescent. This represents an immense simplification and is one of the main reasons for the efficiency of our method.

For the Abelian theory considered in this work, see Sec. 2, we obtain these Δ -inserted 1PI Green functions at the 4-loop level as

$$i\Delta \cdot \Gamma|_{B_\mu(-p)c(p)}^4 = \frac{g^8}{(16\pi^2)^4} \left[\delta \widehat{X}_{BB}^{(4)} \widehat{p}^2 \bar{p}^\mu + \left(\delta \overline{X}_{BB}^{(4)} + \mathcal{F}_{BB}^{4,\text{break}} \right) \bar{p}^2 \bar{p}^\mu \right], \quad (4.24)$$

$$i\Delta \cdot \Gamma|_{\psi_j(p_2)\bar{\psi}_i(p_1)c(q)}^4 = \frac{g^9}{(16\pi^2)^4} (\mathcal{Y}_R)_{ik} \left(\delta \overline{X}_{\bar{\psi}\psi,kj}^{(4)} + \mathcal{F}_{\bar{\psi}\psi,kj}^{4,\text{break}} \right) (\bar{p}_1 + \bar{p}_2) \mathbb{P}_R, \quad (4.25)$$

$$i\Delta \cdot \Gamma|_{B_\nu(p_2)B_\mu(p_1)c(q)}^4 = 0, \quad (4.26)$$

⁷Here, we dropped the subscript “subren”. Note that Γ_{subren} denotes the subnormalised effective quantum action in D dimensions which, in contrast to Γ_{DReg} , does not include the genuine 4-loop counterterms.

$$i\Delta \cdot \Gamma|_{B_\rho(p_3)B_\nu(p_2)B_\mu(p_1)c(q)}^4 = \frac{g^{10}}{(16\pi^2)^4} \left(\delta\bar{X}_{BBBB}^{(4)} + \mathcal{F}_{BBBB}^{4,\text{break}} \right) \times (\bar{p}_1 + \bar{p}_2 + \bar{p}_3)_\sigma (\bar{\eta}^{\mu\nu} \bar{\eta}^{\rho\sigma} + \bar{\eta}^{\mu\rho} \bar{\eta}^{\nu\sigma} + \bar{\eta}^{\mu\sigma} \bar{\eta}^{\nu\rho}), \quad (4.27)$$

with divergent counterterm coefficients as defined in Eqs. (4.10) to (4.13). Our explicit analytical results for the finite counterterm coefficients are provided in App. B.

Note that we do not consider the two power-counting divergent 1PI Green functions

$$i\Delta \cdot \Gamma|_{\psi_j(p_3)\bar{\psi}_i(p_2)B_\mu(p_1)c(q)}^4 \equiv 0, \quad (4.28)$$

$$i\Delta \cdot \Gamma|_{B_\sigma(p_4)B_\rho(p_3)B_\nu(p_2)B_\mu(p_1)c(q)}^4 \equiv 0, \quad (4.29)$$

as they vanish identically. In the Abelian theory studied here, this results from a cancellation of the leading power-counting term in the respective integrands. For the latter Green function, see Eq. (4.29), this also follows from renormalisability arguments, as discussed in Refs. [25, 33].

Indeed, these Green functions fully capture the breaking of BRST symmetry at the 4-loop level, both divergent and finite, as reflected by the breaking of the Slavnov-Taylor identity according to Eq. (4.19). Consequently, the full 4-loop breaking of BRST symmetry can be derived as

$$\begin{aligned} (\Delta \cdot \Gamma)^4 &= \frac{g^8}{(16\pi^2)^4} \int d^D x \left\{ \delta\hat{X}_{BB}^{(4)} c\hat{\partial}^2 \bar{\partial}^\mu \bar{B}_\mu + \left[\delta\bar{X}_{BB}^{(4)} + \mathcal{F}_{BB}^{4,\text{break}} \right] c\bar{\partial}^2 \bar{\partial}^\mu \bar{B}_\mu \right. \\ &\quad + g^2 \left[\delta\bar{X}_{BBBB}^{(4)} + \mathcal{F}_{BBBB}^{4,\text{break}} \right] \frac{1}{2} c\bar{\partial}_\mu (\bar{B}^\mu \bar{B}_\nu \bar{B}^\nu) \\ &\quad \left. + g\mathcal{Y}_{R,ik} \left[\delta\bar{X}_{\bar{\psi}\psi,kj}^{(4)} + \mathcal{F}_{\bar{\psi}\psi,kj}^{4,\text{break}} \right] c\bar{\partial}_\mu (\bar{\psi}_i \bar{\gamma}^\mu \mathbb{P}_R \psi_j) \right\} + \mathcal{O}(\cdot), \end{aligned} \quad (4.30)$$

omitting finite evanescent terms. From this result, we obtain Δ_{ct}^4 via Eq. (4.23).

Using Eq. (4.20), we can first verify that the divergent contributions of Δ_{ct}^4 indeed correctly reproduce the BRST-breaking part of the singular counterterm action, given in Eq. (4.16), serving as the aforementioned consistency check. Second, and more important, we can finally derive the finite, symmetry-restoring counterterms from the finite contributions of Δ_{ct}^4 , which are discussed in the following subsection.

4.3 Four-Loop Finite Symmetry-Restoring Counterterms

From the finite contributions to the BRST breaking in Eq. (4.30), we ultimately derive the finite, symmetry-restoring counterterms at the 4-loop level. Using Eqs. (4.20) and (4.23), we obtain

$$\begin{aligned} S_{\text{fct}}^4 &= \frac{g^8}{(16\pi^2)^4} \int d^4 x \left\{ \mathcal{F}_{BB}^{4,\text{break}} \frac{1}{2} \bar{B}_\mu \bar{\partial}^2 \bar{B}^\mu + g^2 \mathcal{F}_{BBBB}^{4,\text{break}} \frac{1}{8} \bar{B}_\mu \bar{B}^\mu \bar{B}_\nu \bar{B}^\nu \right. \\ &\quad \left. + \mathcal{F}_{\bar{\psi}\psi,ij}^{4,\text{break}} \bar{\psi}_i i\bar{\not{\partial}} \mathbb{P}_R \psi_j \right\}, \end{aligned} \quad (4.31)$$

where our explicit, analytical results for the finite counterterm coefficients in terms of the hypercharge matrix and Riemann zeta values are provided in App. B. This is the main result of this paper.

where the upper left block corresponds to the hypercharges of the right-handed fermions and the lower right block to the hypercharges of the charge-conjugated left-handed fermions. Clearly, this matrix satisfies the anomaly cancellation condition Eq. (2.4). Consistent with the SM hypercharges, it also fulfills the gauge-gravitational anomaly cancellation condition, $\text{Tr}(\mathcal{Y}_R) = 0$, and yields $\text{Tr}(\mathcal{Y}_R^2) = 10$. The latter reflects the fact that all three generations are combined into a single multiplet, and is associated with the normalisation factor of $\sqrt{5/3}$ for the hypercharge gauge coupling in the context of Grand Unified Theories.

Using the explicit Standard Model hypercharges $\mathcal{Y}_R^{\text{SM}}$, see Eq. (4.33), and plugging them into the finite counterterm coefficients in Eqs. (B.10), (B.13) and (B.21), we obtain

$$\begin{aligned}
S_{\text{fct}}^4 \Big|_{\mathcal{Y}_R = \mathcal{Y}_R^{\text{SM}}} &= \frac{g^8}{(16\pi^2)^4} \int d^4x \left\{ \mathcal{F}_{BB}^{4,\text{SM}} \frac{1}{2} \overline{B}_\mu \overline{\partial}^2 \overline{B}^\mu + g^2 \mathcal{F}_{BBBB}^{4,\text{SM}} \frac{1}{8} \overline{B}_\mu \overline{B}^\mu \overline{B}_\nu \overline{B}^\nu \right. \\
&\quad + \mathcal{F}_{\overline{e}e}^{4,\text{SM}} \overline{e}_{R_I} i \overline{\not{\partial}} e_{R_I} + \mathcal{F}_{\overline{u}u}^{4,\text{SM}} \overline{u}_{R_I}^i i \overline{\not{\partial}} u_{R_I}^i + \mathcal{F}_{\overline{d}d}^{4,\text{SM}} \overline{d}_{R_I}^i i \overline{\not{\partial}} d_{R_I}^i \\
&\quad \left. + \mathcal{F}_{\overline{L}L}^{4,\text{SM}} (\overline{L}_{L_I})^C i \overline{\not{\partial}} (L_{L_I})^C + \mathcal{F}_{\overline{Q}Q}^{4,\text{SM}} (\overline{Q}_{L_I}^i)^C i \overline{\not{\partial}} (Q_{L_I}^i)^C \right\}, \quad (4.34)
\end{aligned}$$

for the 4-loop finite, symmetry-restoring counterterms, with explicit coefficients given by

$$\begin{aligned}
\mathcal{F}_{BB}^{4,\text{SM}} &= \frac{105574465087}{604661760} + \frac{2665684621}{6998400} \zeta(3) - \frac{499349}{174960} \zeta(4) - \frac{99009133}{209952} \zeta(5) \approx 140.38, \\
\mathcal{F}_{BBBB}^{4,\text{SM}} &= \frac{1740074889071}{27209779200} - \frac{3393600941}{7873200} \zeta(3) + \frac{151740709}{3149280} \zeta(4) - \frac{50011855}{944784} \zeta(5) \approx -456.91, \\
\mathcal{F}_{\overline{e}e}^{4,\text{SM}} &= \frac{27665962754029}{75582720000} + \frac{3480124631}{17496000} \zeta(3) + \frac{211030883}{583200} \zeta(4) - \frac{20725669}{19440} \zeta(5) \approx -108.73, \\
\mathcal{F}_{\overline{u}u}^{4,\text{SM}} &= \frac{39860981881231}{680244480000} + \frac{22394315941}{88573500} \zeta(3) + \frac{66753553}{1312200} \zeta(4) - \frac{231672547}{787320} \zeta(5) \approx 112.46, \\
\mathcal{F}_{\overline{d}d}^{4,\text{SM}} &= \frac{2388867184943}{340122240000} - \frac{67097069}{1417176000} \zeta(3) + \frac{291946387}{5248800} \zeta(4) - \frac{93959699}{1574640} \zeta(5) \approx 5.29, \\
\mathcal{F}_{\overline{L}L}^{4,\text{SM}} &= \frac{62763071106811}{4837294080000} + \frac{144119506409}{1119744000} \zeta(3) + \frac{619731137}{37324800} \zeta(4) - \frac{34588759}{311040} \zeta(5) \approx 70.35, \\
\mathcal{F}_{\overline{Q}Q}^{4,\text{SM}} &= \frac{72769737196819}{43535646720000} - \frac{437815601831}{90699264000} \zeta(3) + \frac{7110059113}{335923200} \zeta(4) - \frac{476640839}{25194240} \zeta(5) \approx -0.84.
\end{aligned}$$

5 Conclusions

In this work, we successfully performed the first 4-loop renormalisation of an Abelian chiral gauge theory within the BMHV scheme of DReg, providing a fully self-consistent and systematic treatment of γ_5 . We computed the complete counterterm action, including both singular and finite, symmetry-restoring counterterms. In particular, we highlight the finite, symmetry-restoring counterterm action in Eq. (4.31) as a key result of our work. The feasibility of this calculation relied heavily on our efficient methodology and optimised computational framework.

In contrast to previous studies at lower loop orders ($L \leq 3$), no new field monomials emerge in the BRST-breaking contribution to the singular counterterm action at 4 loops. The same holds for the finite, symmetry-restoring counterterms, where this outcome was in fact anticipated. The absence of new field monomials is due to the non-existence of evanescent gauge and Yukawa interactions, as well as constraints from power-counting and renormalisability. The primary difference at the 4-loop order is the increased complexity of

the counterterm coefficients. Thus, we have demonstrated that the complete counterterm action can be expressed in a relatively compact form, even at the 4-loop level, amenable to a straight-forward computer implementation.

In order to perform this calculation, we developed an efficient, automated computational setup. We implemented various optimised algorithms in a `FORM` program, including an efficient implementation of the BMHV algebra and a dedicated procedure for handling γ -matrices. Specifically, we derived and implemented a factorisation of γ -traces, decomposing every trace into an evanescent and a 4-dimensional part. This allows us to use well-established and highly efficient γ -trace algorithms, even within the framework of the BMHV scheme. Additionally, we implemented an efficient algorithm for the reduction of vacuum bubble tensor integrals employing the orbit partition approach. Furthermore, we have systematically applied a concise procedure for symmetry restoration based on the regularised quantum action principle of `DReg`, as established in earlier work. Overall, this project required the calculation of various 4-loop 1PI Green functions, some of which involved billions of terms per Feynman diagram in intermediate steps. The successful execution of these computations not only demonstrates the practical feasibility of 4-loop calculations in the BMHV scheme but also serves as a validation of our computational framework.

The successful application of the BMHV scheme at the 4-loop order demonstrated in this work suggests the suitability of this framework for automated, self-consistent, multi-loop computations in the Standard Model and beyond. This sets the computational stage for more precise calculations of electroweak observables, addressing the increasingly stringent precision requirements of modern experiments.

Acknowledgments

D.S. and M.W. acknowledge financial support by the German Science Foundation DFG, grant STO 876/8-1,2. We would like to thank Amon Ilakovac and Paul Kühler for their insightful ideas and stimulating discussions. Additionally, we are grateful to Ben Ruijl for valuable discussions on the tensor reduction and to York Schroeder for his help with the 4-loop tadpole master integrals, in particular for providing their numerical solutions to perform consistency checks. Furthermore, we thank Joshua Davies, Takahiro Ueda and Jos Vermaseren for discussions and advice regarding `FORM` internal parameter setups. We extend our gratitude to the Centre for Information Services and High Performance Computing [Zentrum für Informationsdienste und Hochleistungsrechnen (ZIH)] TU Dresden for providing its facilities for high-performance calculations, and particularly thank Ulf Markwardt for his support. Finally, M.W. gratefully acknowledges funding from the Graduate Academy of TU Dresden for a three-month research stay at the University of Regensburg, during which a substantial part of this work was carried out.

All Feynman diagrams in this paper have been illustrated using `JaxoDraw` [70].

A Derivation of the γ -Trace Factorisation in D Dimensions

In this Appendix, we discuss the proof of the factorisation of γ -traces in D dimensions within the BMHV scheme. In order to see that Eq. (3.12) holds, we consider all three occurring traces individually. Further, we focus on the case $\mathbb{A} = \mathbb{1}$ and provide arguments for the generalisation to $\mathbb{A} \in \{\mathbb{1}, \gamma_5, \mathbb{P}_L, \mathbb{P}_R\}$ below.

We begin with the 4-dimensional traces $\text{Tr}(\bar{\gamma}^{\mu_1} \dots \bar{\gamma}^{\mu_n} \mathbb{1})$ for which we obtain

$$\begin{aligned}
\text{Tr}(\bar{\gamma}^{\mu_1} \dots \bar{\gamma}^{\mu_n}) &= \text{Tr}(\bar{\gamma}^{\mu_2} \dots \bar{\gamma}^{\mu_n} \bar{\gamma}^{\mu_1}) = \text{Tr}\left(\frac{1}{2}\{\bar{\gamma}^{\mu_1}, \bar{\gamma}^{\mu_2} \dots \bar{\gamma}^{\mu_n}\}\right) \\
&= \sum_{k=2}^n (-1)^k \bar{\eta}^{\mu_1 \mu_k} \text{Tr}(\bar{\gamma}^{\mu_2} \dots \bar{\gamma}^{\mu_{k-1}} \bar{\gamma}^{\mu_{k+1}} \dots \bar{\gamma}^{\mu_n}) \\
&= \sum_{k=1}^{(n-1)!!} (-1)^{\sigma_k(1, \dots, n)} \bar{\eta}^{\mu_{\sigma_k(1)} \mu_{\sigma_k(2)}} \dots \bar{\eta}^{\mu_{\sigma_k(n-1)} \mu_{\sigma_k(n)}} \text{Tr}(\mathbb{1}) \\
&= 4 \sum_{k=1}^{(n-1)!!} (-1)^{\sigma_k(1, \dots, n)} \bar{\eta}^{\mu_{\sigma_k(1)} \mu_{\sigma_k(2)}} \dots \bar{\eta}^{\mu_{\sigma_k(n-1)} \mu_{\sigma_k(n)}},
\end{aligned} \tag{A.1}$$

which is a well-known formula. Here, we used cyclicity of the trace in the first line, evaluated the anticommutator in the second line (see Eq. (3.6)), went to the third line via recursion and used Eq. (3.8) in the last step. Further, we have $(n-1)!! = n!/(2^{n/2}(n/2)!)$, as well as

$$(-1)^{\sigma_k(1, \dots, n)} = \begin{cases} 1, & \text{for even permutations of } \{1, \dots, n\}, \\ -1, & \text{for odd permutations of } \{1, \dots, n\}. \end{cases} \tag{A.2}$$

Similarly, for the evanescent γ -traces, we find

$$\begin{aligned}
\text{Tr}(\hat{\gamma}^{\nu_1} \dots \hat{\gamma}^{\nu_m}) &= \sum_{k=2}^m (-1)^k \hat{\eta}^{\nu_1 \nu_k} \text{Tr}(\hat{\gamma}^{\nu_2} \dots \hat{\gamma}^{\nu_{k-1}} \hat{\gamma}^{\nu_{k+1}} \dots \hat{\gamma}^{\nu_m}) \\
&= 4 \sum_{k=1}^{(m-1)!!} (-1)^{\sigma_k(1, \dots, m)} \hat{\eta}^{\nu_{\sigma_k(1)} \nu_{\sigma_k(2)}} \dots \hat{\eta}^{\nu_{\sigma_k(m-1)} \nu_{\sigma_k(m)}}.
\end{aligned} \tag{A.3}$$

Finally, the LHS of Eq. (3.12) evaluates to

$$\begin{aligned}
&\text{Tr}(\hat{\gamma}^{\nu_1} \dots \hat{\gamma}^{\nu_m} \bar{\gamma}^{\mu_1} \dots \bar{\gamma}^{\mu_n}) \\
&= (-1)^{n+m} \text{Tr}(\hat{\gamma}^{\nu_2} \dots \hat{\gamma}^{\nu_m} \hat{\gamma}^{\nu_1} \bar{\gamma}^{\mu_2} \dots \bar{\gamma}^{\mu_n} \bar{\gamma}^{\mu_1}) = \text{Tr}(\hat{\gamma}^{\nu_2} \dots \hat{\gamma}^{\nu_m} \hat{\gamma}^{\nu_1} \bar{\gamma}^{\mu_2} \dots \bar{\gamma}^{\mu_n} \bar{\gamma}^{\mu_1}) \\
&= \text{Tr}\left(\frac{1}{2}\{\hat{\gamma}^{\nu_1}, \hat{\gamma}^{\nu_2} \dots \hat{\gamma}^{\nu_m}\} \frac{1}{2}\{\bar{\gamma}^{\mu_1}, \bar{\gamma}^{\mu_2} \dots \bar{\gamma}^{\mu_n}\}\right) \\
&= \sum_{k=2}^m \sum_{l=2}^n (-1)^k (-1)^l \hat{\eta}^{\nu_1 \nu_k} \bar{\eta}^{\mu_1 \mu_l} \text{Tr}(\hat{\gamma}^{\nu_2} \dots \hat{\gamma}^{\nu_{l-1}} \hat{\gamma}^{\nu_{l+1}} \dots \hat{\gamma}^{\nu_m} \bar{\gamma}^{\mu_2} \dots \bar{\gamma}^{\mu_{k-1}} \bar{\gamma}^{\mu_{k+1}} \dots \bar{\gamma}^{\mu_n}) \\
&= \sum_{k=1}^{(m-1)!!} (-1)^{\sigma_k(1, \dots, m)} \hat{\eta}^{\nu_{\sigma_k(1)} \nu_{\sigma_k(2)}} \dots \hat{\eta}^{\nu_{\sigma_k(m-1)} \nu_{\sigma_k(m)}} \\
&\quad \times \sum_{l=1}^{(n-1)!!} (-1)^{\sigma_l(1, \dots, n)} \bar{\eta}^{\mu_{\sigma_l(1)} \mu_{\sigma_l(2)}} \dots \bar{\eta}^{\mu_{\sigma_l(n-1)} \mu_{\sigma_l(n)}} \text{Tr}(\mathbb{1})
\end{aligned} \tag{A.4}$$

$$\begin{aligned}
&= 4 \sum_{k=1}^{(m-1)!!} (-1)^{\sigma_k(1,\dots,m)} \widehat{\eta}^{\nu_{\sigma_k(1)} \nu_{\sigma_k(2)}} \dots \widehat{\eta}^{\nu_{\sigma_k(m-1)} \nu_{\sigma_k(m)}} \\
&\quad \times \sum_{l=1}^{(n-1)!!} (-1)^{\sigma_l(1,\dots,n)} \overline{\eta}^{\mu_{\sigma_l(1)} \mu_{\sigma_l(2)}} \dots \overline{\eta}^{\mu_{\sigma_l(n-1)} \mu_{\sigma_l(n)}},
\end{aligned}$$

where we used cyclicity of the trace and $\{\overline{\gamma}^\mu, \widehat{\gamma}^\nu\} = 0$, as well as the fact that only traces with even n and m give rise to non-vanishing contributions in the second line. Rewriting the resulting expression using the anticommutator leads to the third line, while the evaluation of this anticommutator results in the fourth line. We again arrive at the penultimate step via recursion and obtain the last equality by using (3.8). Comparing Eqs. (A.1) and (A.3) with Eq. (A.4) leads to the desired result given in Eq. (3.12) for $\mathbb{A} = \mathbb{1}$. Evidently, the additional factor of $1/4$ on the RHS of Eq. (3.12) comes from the fact that ultimately there are two traces of the identity, whereas there is only one on the LHS, which needs to be taken into account.

This result can be generalised to $\mathbb{A} \in \{\mathbb{1}, \gamma_5, \mathbb{P}_L, \mathbb{P}_R\}$, using the (anti-)commutation relations of γ_5 given in Eq. (3.7) in the first two steps of the treatment of the LHS of Eq. (3.12) for general \mathbb{A} (cf. Eq. (A.4) for $\mathbb{A} = \mathbb{1}$), as well as

$$\begin{aligned}
\text{Tr}(\gamma_5) &= 0, \\
\text{Tr}(\overline{\gamma}^\mu \overline{\gamma}^\nu \gamma_5) &= 0, \\
\text{Tr}(\overline{\gamma}^{\mu_1} \dots \overline{\gamma}^{\mu_{2n+1}} \gamma_5) &= 0,
\end{aligned} \tag{A.5}$$

and, for $n = 4$,

$$\text{Tr}(\gamma_5 \overline{\gamma}^\mu \overline{\gamma}^\nu \overline{\gamma}^\rho \overline{\gamma}^\sigma) = -4i \varepsilon^{\mu\nu\rho\sigma}, \tag{A.6}$$

while even $n \geq 6$ can be treated recursively using

$$\overline{\gamma}^\mu \overline{\gamma}^\nu \overline{\gamma}^\rho = \overline{\eta}^{\mu\nu} \gamma_5 \overline{\gamma}^\rho - \overline{\eta}^{\mu\rho} \gamma_5 \overline{\gamma}^\nu + \overline{\eta}^{\nu\rho} \gamma_5 \overline{\gamma}^\mu - i \varepsilon^{\mu\nu\rho\sigma} \overline{\gamma}_\sigma. \tag{A.7}$$

B Explicit Results for the Four-Loop Coefficients

In this section, we present the explicit results for all 4-loop coefficients used in Sec. 4. Additionally, we provide the ancillary file `BMHVAbelian4LoopResults.m`, which contains the full set of Green functions shown in Eqs. (4.3) to (4.7) and (4.24) to (4.29), along with all coefficients listed below. We first present the counterterm coefficients for pure gauge boson contributions, and then proceed to the fermionic contributions.

Gauge Boson Four-Loop Coefficients: We begin with the coefficients associated with the divergent, BRST-invariant bilinear gauge boson counterterm, see Eq. (4.8),

$$\begin{aligned}
\mathcal{A}_{BB}^{4,\text{inv}} &= \left(\frac{1322627}{97200} + \frac{4019 \zeta(3)}{675} \right) \text{Tr}(\mathcal{Y}_R^8) \\
&\quad + \left(\frac{104077}{116640} - \frac{1058 \zeta(3)}{2025} \right) \text{Tr}(\mathcal{Y}_R^6) \text{Tr}(\mathcal{Y}_R^2) \\
&\quad + \left(\frac{537133}{583200} + \frac{34 \zeta(3)}{3} \right) \text{Tr}(\mathcal{Y}_R^4)^2 + \frac{4111}{145800} \text{Tr}(\mathcal{Y}_R^4) \text{Tr}(\mathcal{Y}_R^2)^2,
\end{aligned} \tag{B.1}$$

$$\mathcal{B}_{BB}^{4,\text{inv}} = -\frac{13}{45} \text{Tr}(\mathcal{Y}_R^8) - \frac{371}{1080} \text{Tr}(\mathcal{Y}_R^6) \text{Tr}(\mathcal{Y}_R^2) - \frac{1607}{3240} \text{Tr}(\mathcal{Y}_R^4)^2 - \frac{707}{14580} \text{Tr}(\mathcal{Y}_R^4) \text{Tr}(\mathcal{Y}_R^2)^2, \quad (\text{B.2})$$

$$\mathcal{C}_{BB}^{4,\text{inv}} = \frac{1}{54} \text{Tr}(\mathcal{Y}_R^6) \text{Tr}(\mathcal{Y}_R^2) + \frac{1}{162} \text{Tr}(\mathcal{Y}_R^4)^2 - \frac{23}{486} \text{Tr}(\mathcal{Y}_R^4) \text{Tr}(\mathcal{Y}_R^2)^2. \quad (\text{B.3})$$

Next, we present the coefficients for the divergent, BRST-breaking and evanescent counterterm that is bilinear in gauge bosons, see Eq. (4.10),

$$\begin{aligned} \widehat{\mathcal{A}}_{BB}^{4,\text{break}} &= -\left(\frac{389961509}{15552000} + \frac{67\pi^4}{9000} + \frac{1119401\zeta(3)}{27000} - \frac{4079\zeta(5)}{45}\right) \text{Tr}(\mathcal{Y}_R^8) \\ &\quad - \left(\frac{19047839}{11664000} + \frac{659\pi^4}{40500} - \frac{8471\zeta(3)}{6750}\right) \text{Tr}(\mathcal{Y}_R^6) \text{Tr}(\mathcal{Y}_R^2) \\ &\quad - \left(\frac{131895011}{11664000} + \frac{27512\zeta(3)}{675} - \frac{2954\zeta(5)}{45}\right) \text{Tr}(\mathcal{Y}_R^4)^2 \\ &\quad - \frac{102163}{1749600} \text{Tr}(\mathcal{Y}_R^4) \text{Tr}(\mathcal{Y}_R^2)^2, \end{aligned} \quad (\text{B.4})$$

$$\begin{aligned} \widehat{\mathcal{B}}_{BB}^{4,\text{break}} &= -\left(\frac{582931}{259200} + \frac{67\zeta(3)}{150}\right) \text{Tr}(\mathcal{Y}_R^8) + \left(\frac{8263}{12960} - \frac{659\zeta(3)}{675}\right) \text{Tr}(\mathcal{Y}_R^6) \text{Tr}(\mathcal{Y}_R^2) \\ &\quad + \frac{361}{2700} \text{Tr}(\mathcal{Y}_R^4)^2 + \frac{1399}{19440} \text{Tr}(\mathcal{Y}_R^4) \text{Tr}(\mathcal{Y}_R^2)^2, \end{aligned} \quad (\text{B.5})$$

$$\widehat{\mathcal{C}}_{BB}^{4,\text{break}} = \frac{1231}{4320} \text{Tr}(\mathcal{Y}_R^8) + \frac{83}{540} \text{Tr}(\mathcal{Y}_R^6) \text{Tr}(\mathcal{Y}_R^2) + \frac{7}{1080} \text{Tr}(\mathcal{Y}_R^4)^2 + \frac{\text{Tr}(\mathcal{Y}_R^4) \text{Tr}(\mathcal{Y}_R^2)^2}{27}, \quad (\text{B.6})$$

$$\widehat{\mathcal{D}}_{BB}^{4,\text{break}} = -\frac{\text{Tr}(\mathcal{Y}_R^8)}{72}, \quad (\text{B.7})$$

followed by the coefficients for the divergent, BRST-breaking and 4-dimensional counterterm that is bilinear in gauge bosons, see Eq. (4.11),

$$\begin{aligned} \overline{\mathcal{A}}_{BB}^{4,\text{break}} &= -\left(\frac{2353}{16200} - \frac{4\zeta(3)}{225}\right) \text{Tr}(\mathcal{Y}_R^8) - \left(\frac{22999}{38880} + \frac{34\zeta(3)}{675}\right) \text{Tr}(\mathcal{Y}_R^6) \text{Tr}(\mathcal{Y}_R^2) \\ &\quad - \frac{2507}{64800} \text{Tr}(\mathcal{Y}_R^4)^2 - \frac{10327}{1166400} \text{Tr}(\mathcal{Y}_R^4) \text{Tr}(\mathcal{Y}_R^2)^2, \end{aligned} \quad (\text{B.8})$$

$$\overline{\mathcal{B}}_{BB}^{4,\text{break}} = \frac{\text{Tr}(\mathcal{Y}_R^8)}{1080} + \frac{13}{3240} \text{Tr}(\mathcal{Y}_R^6) \text{Tr}(\mathcal{Y}_R^2) + \frac{\text{Tr}(\mathcal{Y}_R^4)^2}{720} + \frac{449}{19440} \text{Tr}(\mathcal{Y}_R^4) \text{Tr}(\mathcal{Y}_R^2)^2. \quad (\text{B.9})$$

The coefficient of the finite, symmetry-restoring bilinear gauge boson counterterm reads

$$\begin{aligned} \mathcal{F}_{BB}^{4,\text{break}} &= \left(\frac{403759}{25920} + \frac{\pi^4}{3375} + \frac{30113\zeta(3)}{4500} - \frac{403\zeta(5)}{45}\right) \text{Tr}(\mathcal{Y}_R^8) \\ &\quad + \left(\frac{4525151}{11664000} - \frac{17\pi^4}{20250} - \frac{15569\zeta(3)}{40500}\right) \text{Tr}(\mathcal{Y}_R^6) \text{Tr}(\mathcal{Y}_R^2) \\ &\quad + \left(\frac{38768057}{7776000} + \frac{12061\zeta(3)}{900} - \frac{713\zeta(5)}{45}\right) \text{Tr}(\mathcal{Y}_R^4)^2 \\ &\quad - \frac{4240349}{69984000} \text{Tr}(\mathcal{Y}_R^4) \text{Tr}(\mathcal{Y}_R^2)^2. \end{aligned} \quad (\text{B.10})$$

For the quartic gauge boson counterterm, the coefficients for the divergent, BRST-breaking and 4-dimensional contribution, see Eq. (4.12), are provided by

$$\begin{aligned} \overline{\mathcal{A}}_{BBBB}^{4,\text{break}} &= \left(\frac{1742}{2025} + \frac{8\zeta(3)}{225} \right) \text{Tr}(\mathcal{Y}_R^{10}) + \left(\frac{75677}{48600} + \frac{128\zeta(3)}{135} \right) \text{Tr}(\mathcal{Y}_R^8) \text{Tr}(\mathcal{Y}_R^2) \\ &+ \frac{12359}{3240} \text{Tr}(\mathcal{Y}_R^6) \text{Tr}(\mathcal{Y}_R^4) - \frac{3539}{291600} \text{Tr}(\mathcal{Y}_R^6) \text{Tr}(\mathcal{Y}_R^2)^2 - \frac{998}{1215} \text{Tr}(\mathcal{Y}_R^5)^2 \\ &- \frac{407}{4860} \text{Tr}(\mathcal{Y}_R^4)^2 \text{Tr}(\mathcal{Y}_R^2), \end{aligned} \quad (\text{B.11})$$

$$\begin{aligned} \overline{\mathcal{B}}_{BBBB}^{4,\text{break}} &= -\frac{1}{270} \text{Tr}(\mathcal{Y}_R^{10}) - \frac{19}{810} \text{Tr}(\mathcal{Y}_R^8) \text{Tr}(\mathcal{Y}_R^2) - \frac{1}{108} \text{Tr}(\mathcal{Y}_R^6) \text{Tr}(\mathcal{Y}_R^4) \\ &- \frac{347}{4860} \text{Tr}(\mathcal{Y}_R^6) \text{Tr}(\mathcal{Y}_R^2)^2 - \frac{2}{3} \text{Tr}(\mathcal{Y}_R^4)^2 \text{Tr}(\mathcal{Y}_R^2), \end{aligned} \quad (\text{B.12})$$

while the coefficient of the finite, symmetry-restoring contribution is given by

$$\begin{aligned} \mathcal{F}_{BBBB}^{4,\text{break}} &= -\left(\frac{1123939}{18000} - \frac{2\pi^4}{3375} + \frac{43376\zeta(3)}{1125} - \frac{392\zeta(5)}{9} \right) \text{Tr}(\mathcal{Y}_R^{10}) \\ &+ \left(\frac{3544039}{2916000} + \frac{32\pi^4}{2025} - \frac{599\zeta(3)}{2025} \right) \text{Tr}(\mathcal{Y}_R^8) \text{Tr}(\mathcal{Y}_R^2) \\ &- \left(\frac{666463}{388800} + \frac{10888\zeta(3)}{675} + \frac{40\zeta(5)}{9} \right) \text{Tr}(\mathcal{Y}_R^6) \text{Tr}(\mathcal{Y}_R^4) \\ &+ \frac{6224207}{17496000} \text{Tr}(\mathcal{Y}_R^6) \text{Tr}(\mathcal{Y}_R^2)^2 + \frac{93341}{291600} \text{Tr}(\mathcal{Y}_R^4)^2 \text{Tr}(\mathcal{Y}_R^2) \\ &+ \left(\frac{730379}{72900} + \frac{7922\zeta(3)}{675} - \frac{536\zeta(5)}{15} \right) \text{Tr}(\mathcal{Y}_R^5)^2. \end{aligned} \quad (\text{B.13})$$

Fermion Four-Loop Coefficients: Analogous to the case of the gauge boson contributions, we proceed to list all coefficients for the fermionic 4-loop counterterms. We begin with those for the divergent fermionic contributions, see Eq. (4.9),

$$\begin{aligned} \mathcal{A}_{\psi\bar{\psi},ij}^{4,\text{inv}} &= \left(\frac{156477439}{2592000} + \frac{32773\zeta(3)}{300} - 160\zeta(5) \right) (\mathcal{Y}_R^8)_{ij} \\ &- \left(\frac{14415971}{2592000} + \frac{2357\zeta(3)}{450} \right) \text{Tr}(\mathcal{Y}_R^2) (\mathcal{Y}_R^6)_{ij} \\ &- \left[\left(\frac{28122617}{1555200} - \frac{3104\zeta(3)}{225} \right) \text{Tr}(\mathcal{Y}_R^4) - \frac{3213671}{11664000} \text{Tr}(\mathcal{Y}_R^2)^2 \right] (\mathcal{Y}_R^4)_{ij} \\ &- \left(\frac{8177}{2880} - \frac{264\zeta(3)}{25} \right) \text{Tr}(\mathcal{Y}_R^5) (\mathcal{Y}_R^3)_{ij} \\ &- \left[\left(\frac{2252129}{777600} - \frac{547\zeta(3)}{450} \right) \text{Tr}(\mathcal{Y}_R^6) + \frac{66841}{11664000} \text{Tr}(\mathcal{Y}_R^2)^3 \right. \\ &+ \left. \left(\frac{161755}{186624} + \frac{1069\zeta(3)}{450} \right) \text{Tr}(\mathcal{Y}_R^4) \text{Tr}(\mathcal{Y}_R^2) \right] (\mathcal{Y}_R^2)_{ij} \\ &+ \left[\left(\frac{49367}{9600} - \frac{2\zeta(3)}{5} \right) \text{Tr}(\mathcal{Y}_R^7) \right. \\ &+ \left. \left(\frac{1271}{1440} - \frac{257\zeta(3)}{75} \right) \text{Tr}(\mathcal{Y}_R^5) \text{Tr}(\mathcal{Y}_R^2) \right] (\mathcal{Y}_R)_{ij}, \end{aligned} \quad (\text{B.14})$$

$$\begin{aligned}
\mathcal{B}_{\psi\bar{\psi},ij}^{4,\text{inv}} &= \frac{29063}{4800}(\mathcal{Y}_R^8)_{ij} - \frac{147353}{43200}\text{Tr}(\mathcal{Y}_R^2)(\mathcal{Y}_R^6)_{ij} \\
&\quad - \left(\frac{1}{90}\text{Tr}(\mathcal{Y}_R^4) - \frac{43811}{64800}\text{Tr}(\mathcal{Y}_R^2)^2 \right) (\mathcal{Y}_R^4)_{ij} + \frac{299}{240}\text{Tr}(\mathcal{Y}_R^5)(\mathcal{Y}_R^3)_{ij} \\
&\quad - \left(\frac{611}{12960}\text{Tr}(\mathcal{Y}_R^6) - \frac{13429}{38880}\text{Tr}(\mathcal{Y}_R^4)\text{Tr}(\mathcal{Y}_R^2) - \frac{157}{194400}\text{Tr}(\mathcal{Y}_R^2)^3 \right) (\mathcal{Y}_R^2)_{ij} \\
&\quad - \left(\frac{37}{480}\text{Tr}(\mathcal{Y}_R^7) + \frac{191}{360}\text{Tr}(\mathcal{Y}_R^5)\text{Tr}(\mathcal{Y}_R^2) \right) (\mathcal{Y}_R)_{ij},
\end{aligned} \tag{B.15}$$

$$\begin{aligned}
\mathcal{C}_{\psi\bar{\psi},ij}^{4,\text{inv}} &= \frac{451}{720}(\mathcal{Y}_R^8)_{ij} - \frac{1057}{2160}\text{Tr}(\mathcal{Y}_R^2)(\mathcal{Y}_R^6)_{ij} \\
&\quad - \left(\frac{7}{432}\text{Tr}(\mathcal{Y}_R^4) - \frac{109}{540}\text{Tr}(\mathcal{Y}_R^2)^2 \right) (\mathcal{Y}_R^4)_{ij} \\
&\quad + \left(\frac{\text{Tr}(\mathcal{Y}_R^6)}{216} + \frac{\text{Tr}(\mathcal{Y}_R^4)\text{Tr}(\mathcal{Y}_R^2)}{432} + \frac{\text{Tr}(\mathcal{Y}_R^2)^3}{3240} \right) (\mathcal{Y}_R^2)_{ij},
\end{aligned} \tag{B.16}$$

$$\mathcal{D}_{\psi\bar{\psi},ij}^{4,\text{inv}} = \frac{1}{24}(\mathcal{Y}_R^8)_{ij}, \tag{B.17}$$

as well as those in Eq. (4.13),

$$\begin{aligned}
\bar{\mathcal{A}}_{\psi\bar{\psi},ij}^{4,\text{break}} &= - \left(\frac{29481469}{1296000} + \frac{5461}{900}\zeta(3) \right) (\mathcal{Y}_R^8)_{ij} \\
&\quad + \left(\frac{82599047}{7776000} + \frac{2411}{900}\zeta(3) \right) \text{Tr}(\mathcal{Y}_R^2)(\mathcal{Y}_R^6)_{ij} \\
&\quad - \left[\left(\frac{919571}{388800} + \frac{1198}{225}\zeta(3) \right) \text{Tr}(\mathcal{Y}_R^4) + \frac{10432717}{11664000}\text{Tr}(\mathcal{Y}_R^2)^2 \right] (\mathcal{Y}_R^4)_{ij} \\
&\quad + \left(\frac{8233}{14400} - \frac{707}{100}\zeta(3) \right) \text{Tr}(\mathcal{Y}_R^5)(\mathcal{Y}_R^3)_{ij} \\
&\quad + \left[\left(\frac{1194907}{777600} - \frac{23}{90}\zeta(3) \right) \text{Tr}(\mathcal{Y}_R^6) - \frac{22139}{1296000}\text{Tr}(\mathcal{Y}_R^2)^3 \right. \\
&\quad \left. + \left(\frac{41257}{186624} + \frac{335}{108}\zeta(3) \right) \text{Tr}(\mathcal{Y}_R^4)\text{Tr}(\mathcal{Y}_R^2) \right] (\mathcal{Y}_R^2)_{ij} \\
&\quad - \left[\left(\frac{49367}{9600} - \frac{2}{5}\zeta(3) \right) \text{Tr}(\mathcal{Y}_R^7) \right. \\
&\quad \left. + \left(\frac{1271}{1440} - \frac{257}{75}\zeta(3) \right) \text{Tr}(\mathcal{Y}_R^5)\text{Tr}(\mathcal{Y}_R^2) \right] (\mathcal{Y}_R)_{ij},
\end{aligned} \tag{B.18}$$

$$\begin{aligned}
\bar{\mathcal{B}}_{\psi\bar{\psi},ij}^{4,\text{break}} &= - \frac{16609}{7200}(\mathcal{Y}_R^8)_{ij} + \frac{254021}{129600}\text{Tr}(\mathcal{Y}_R^2)(\mathcal{Y}_R^6)_{ij} - \frac{149}{240}\text{Tr}(\mathcal{Y}_R^5)(\mathcal{Y}_R^3)_{ij} \\
&\quad + \left(\frac{121}{810}\text{Tr}(\mathcal{Y}_R^4) - \frac{145091}{194400}\text{Tr}(\mathcal{Y}_R^2)^2 \right) (\mathcal{Y}_R^4)_{ij} \\
&\quad - \left(\frac{719}{12960}\text{Tr}(\mathcal{Y}_R^6) + \frac{107}{864}\text{Tr}(\mathcal{Y}_R^4)\text{Tr}(\mathcal{Y}_R^2) - \frac{2909}{64800}\text{Tr}(\mathcal{Y}_R^2)^3 \right) (\mathcal{Y}_R^2)_{ij} \\
&\quad + \left(\frac{37}{480}\text{Tr}(\mathcal{Y}_R^7) + \frac{191}{360}\text{Tr}(\mathcal{Y}_R^5)\text{Tr}(\mathcal{Y}_R^2) \right) (\mathcal{Y}_R)_{ij},
\end{aligned} \tag{B.19}$$

$$\begin{aligned}
\bar{\mathcal{C}}_{\psi\bar{\psi},ij}^{4,\text{break}} &= -\frac{31}{360}(\mathcal{Y}_R^8)_{ij} + \frac{41}{720}\text{Tr}(\mathcal{Y}_R^2)(\mathcal{Y}_R^6)_{ij} \\
&\quad - \left(\frac{\text{Tr}(\mathcal{Y}_R^4)}{54} + \frac{173}{3240}\text{Tr}(\mathcal{Y}_R^2)^2 \right) (\mathcal{Y}_R^4)_{ij} \\
&\quad + \left(\frac{1}{216}\text{Tr}(\mathcal{Y}_R^6) + \frac{5}{432}\text{Tr}(\mathcal{Y}_R^4)\text{Tr}(\mathcal{Y}_R^2) + \frac{37}{1080}\text{Tr}(\mathcal{Y}_R^2)^3 \right) (\mathcal{Y}_R^2)_{ij}.
\end{aligned} \tag{B.20}$$

Finally, the coefficient of the finite, symmetry-restoring fermionic counterterm is given by

$$\begin{aligned}
\mathcal{F}_{\psi\bar{\psi},ij}^{4,\text{break}} &= - \left(\frac{2296950361}{25920000} - \frac{113\pi^4}{18000} + \frac{3803231}{54000}\zeta(3) - \frac{\zeta(5)}{15} \right) (\mathcal{Y}_R^8)_{ij} \\
&\quad + \left(\frac{887862323}{155520000} + \frac{2411\pi^4}{54000} + \frac{113087}{18000}\zeta(3) \right) \text{Tr}(\mathcal{Y}_R^2)(\mathcal{Y}_R^6)_{ij} \\
&\quad + \left[\left(\frac{33905827}{583200} - \frac{37\pi^4}{3375} + \frac{307901}{6750}\zeta(3) - \frac{7153}{45}\zeta(5) \right) \text{Tr}(\mathcal{Y}_R^4) \right. \\
&\quad \quad \left. + \left(\frac{579755521}{699840000} + \frac{29}{540}\zeta(3) \right) \text{Tr}(\mathcal{Y}_R^2)^2 \right] (\mathcal{Y}_R^4)_{ij} \\
&\quad + \left(\frac{1593257}{172800} - \frac{7\pi^4}{6000} - \frac{729797}{6000}\zeta(3) + \frac{479}{6}\zeta(5) \right) \text{Tr}(\mathcal{Y}_R^5)(\mathcal{Y}_R^3)_{ij} \\
&\quad + \left[\left(\frac{975213329}{46656000} - \frac{1433\pi^4}{81000} + \frac{811729}{27000}\zeta(3) - \frac{1141}{15}\zeta(5) \right) \text{Tr}(\mathcal{Y}_R^6) \right. \\
&\quad \quad \left. + \left(\frac{78192881}{139968000} + \frac{67\pi^4}{1296} + \frac{299}{400}\zeta(3) \right) \text{Tr}(\mathcal{Y}_R^4)\text{Tr}(\mathcal{Y}_R^2) \right. \\
&\quad \quad \left. - \left(\frac{3350431}{25920000} - \frac{37}{540}\zeta(3) \right) \text{Tr}(\mathcal{Y}_R^2)^3 \right] (\mathcal{Y}_R^2)_{ij} \\
&\quad + \left[\left(\frac{42763633}{1728000} + \frac{\pi^4}{150} - \frac{5923}{300}\zeta(3) - \frac{263}{10}\zeta(5) \right) \text{Tr}(\mathcal{Y}_R^7) \right. \\
&\quad \quad \left. - \left(\frac{3833903}{1296000} - \frac{257\pi^4}{4500} + \frac{1261}{1500}\zeta(3) \right) \text{Tr}(\mathcal{Y}_R^5)\text{Tr}(\mathcal{Y}_R^2) \right] (\mathcal{Y}_R)_{ij}.
\end{aligned} \tag{B.21}$$

References

- [1] G. 't Hooft and M. J. G. Veltman, “Regularization and Renormalization of Gauge Fields,” *Nucl. Phys. B*, vol. 44, pp. 189–213, 1972. DOI: 10.1016/0550-3213(72)90279-9.
- [2] P. Breitenlohner and D. Maison, “Dimensionally Renormalized Green’s Functions for Theories with Massless Particles. 1.,” *Commun. Math. Phys.*, vol. 52, p. 39, 1977. DOI: 10.1007/BF01609070.
- [3] P. Breitenlohner and D. Maison, “Dimensionally Renormalized Green’s Functions for Theories with Massless Particles. 2.,” *Commun. Math. Phys.*, vol. 52, p. 55, 1977. DOI: 10.1007/BF01609071.
- [4] P. Breitenlohner and D. Maison, “Dimensional Renormalization and the Action Principle,” *Commun. Math. Phys.*, vol. 52, pp. 11–38, 1977. DOI: 10.1007/BF01609069.

- [5] F. Jegerlehner, “Facts of life with $\gamma(5)$,” *Eur. Phys. J. C*, vol. 18, pp. 673–679, 2001. DOI: 10.1007/s100520100573. arXiv: hep-th/0005255.
- [6] H. Bélusca-Maïto, A. Ilakovac, P. Kühler, M. Mađor-Božinović, D. Stöckinger and M. Weißwange, “Introduction to Renormalization Theory and Chiral Gauge Theories in Dimensional Regularization with Non-Anticommuting γ_5 ,” *Symmetry*, vol. 15, no. 3, p. 622, 2023. DOI: 10.3390/sym15030622. arXiv: 2303.09120 [hep-ph].
- [7] D. Kreimer, “The $\gamma(5)$ Problem and Anomalies: A Clifford Algebra Approach,” *Phys. Lett. B*, vol. 237, pp. 59–62, 1990. DOI: 10.1016/0370-2693(90)90461-E.
- [8] J. G. Korner, D. Kreimer and K. Schilcher, “A Practicable $\gamma(5)$ scheme in dimensional regularization,” *Z. Phys. C*, vol. 54, pp. 503–512, 1992. DOI: 10.1007/BF01559471.
- [9] D. Kreimer, “The Role of $\gamma(5)$ in dimensional regularization,” Dec. 1993. arXiv: hep-ph/9401354.
- [10] S. A. Larin, “The Renormalization of the axial anomaly in dimensional regularization,” *Phys. Lett. B*, vol. 303, pp. 113–118, 1993. DOI: 10.1016/0370-2693(93)90053-K. arXiv: hep-ph/9302240.
- [11] K. G. Chetyrkin and M. F. Zoller, “Three-loop β -functions for top-Yukawa and the Higgs self-interaction in the Standard Model,” *JHEP*, vol. 06, p. 033, 2012. DOI: 10.1007/JHEP06(2012)033. arXiv: 1205.2892 [hep-ph].
- [12] M. F. Zoller, “Top-Yukawa effects on the β -function of the strong coupling in the SM at four-loop level,” *JHEP*, vol. 02, p. 095, 2016. DOI: 10.1007/JHEP02(2016)095. arXiv: 1508.03624 [hep-ph].
- [13] A. V. Bednyakov and A. F. Pikelner, “Four-loop strong coupling beta-function in the Standard Model,” *Phys. Lett. B*, vol. 762, pp. 151–156, 2016. DOI: 10.1016/j.physletb.2016.09.007. arXiv: 1508.02680 [hep-ph].
- [14] C. Poole and A. E. Thomsen, “Weyl Consistency Conditions and γ_5 ,” *Phys. Rev. Lett.*, vol. 123, no. 4, p. 041602, 2019. DOI: 10.1103/PhysRevLett.123.041602. arXiv: 1901.02749 [hep-th].
- [15] J. Davies, F. Herren, C. Poole, M. Steinhauser and A. E. Thomsen, “Gauge Coupling β Functions to Four-Loop Order in the Standard Model,” *Phys. Rev. Lett.*, vol. 124, no. 7, p. 071803, 2020. DOI: 10.1103/PhysRevLett.124.071803. arXiv: 1912.07624 [hep-ph].
- [16] J. Davies, F. Herren and A. E. Thomsen, “General gauge-Yukawa-quartic β -functions at 4-3-2-loop order,” *JHEP*, vol. 01, p. 051, 2022. DOI: 10.1007/JHEP01(2022)051. arXiv: 2110.05496 [hep-ph].
- [17] F. Herren, “Higher-order β -functions in the Standard Model and beyond,” *SciPost Phys. Proc.*, vol. 7, p. 029, 2022. DOI: 10.21468/SciPostPhysProc.7.029. arXiv: 2110.06938 [hep-ph].
- [18] L. Chen, “An observation on Feynman diagrams with axial anomalous subgraphs in dimensional regularization with an anticommuting γ_5 ,” *JHEP*, vol. 2023, no. 11, p. 30, 2023. DOI: 10.1007/JHEP11(2023)030. arXiv: 2304.13814 [hep-ph].
- [19] L. Chen, “A Procedure g_5 anchor to Anchor γ_5 in Feynman Diagrams for the Standard Model,” Sep. 2024. arXiv: 2409.08099 [hep-ph].

- [20] H. Béhusca-Maïto, A. Ilakovac, M. Mador-Božinović and D. Stöckinger, “Dimensional regularization and Breitenlohner-Maison/’t Hooft-Veltman scheme for γ_5 applied to chiral YM theories: full one-loop counterterm and RGE structure,” *JHEP*, vol. 08, no. 08, p. 024, 2020. DOI: 10.1007/JHEP08(2020)024. arXiv: 2004.14398 [hep-ph].
- [21] P. Olgoso Ruiz and L. Vecchi, “Spurious gauge-invariance and γ_5 in Dimensional Regularization,” Jun. 2024. arXiv: 2406.17013 [hep-ph].
- [22] C. P. Martin and D. Sanchez-Ruiz, “Action principles, restoration of BRS symmetry and the renormalization group equation for chiral nonAbelian gauge theories in dimensional renormalization with a nonanticommuting γ_5 ,” *Nucl. Phys. B*, vol. 572, pp. 387–477, 2000. DOI: 10.1016/S0550-3213(99)00453-8. arXiv: hep-th/9905076.
- [23] C. Cornella, F. Feruglio and L. Vecchi, “Gauge invariance and finite counterterms in chiral gauge theories,” *JHEP*, vol. 02, p. 244, 2023. DOI: 10.1007/JHEP02(2023)244. arXiv: 2205.10381 [hep-ph].
- [24] D. Sanchez-Ruiz, “BRS symmetry restoration of chiral Abelian Higgs-Kibble theory in dimensional renormalization with a nonanticommuting γ_5 ,” *Phys. Rev. D*, vol. 68, p. 025 009, 2003. DOI: 10.1103/PhysRevD.68.025009. arXiv: hep-th/0209023.
- [25] P. L. Ebert, P. Kühler, D. Stöckinger and M. Weißwange, “Shedding light on evanescent shadows — Exploration of non-anticommuting γ_5 in Dimensional Regularisation,” *JHEP*, vol. 01, p. 114, 2025. DOI: 10.1007/JHEP01(2025)114. arXiv: 2411.02543 [hep-ph].
- [26] L. Naterop and P. Stoffer, “Low-energy effective field theory below the electroweak scale: one-loop renormalization in the ’t Hooft-Veltman scheme,” *JHEP*, vol. 02, p. 068, 2024. DOI: 10.1007/JHEP02(2024)068. arXiv: 2310.13051 [hep-ph].
- [27] S. Di Noi, R. Gröber, G. Heinrich, J. Lang and M. Vitti, “ γ_5 schemes and the interplay of smeft operators in the higgs-gluon coupling,” *Phys. Rev. D*, vol. 109, no. 9, p. 095 024, 2024. DOI: 10.1103/PhysRevD.109.095024. arXiv: 2310.18221 [hep-ph].
- [28] G. Heinrich, S. Di Noi, R. Gröber, J. Lang, L. Scyboz and M. Vitti, “Subleading operators and γ_5 -scheme dependence in SMEFT for Higgs boson pair production,” *PoS*, vol. LL2024, p. 021, 2024. DOI: 10.22323/1.467.0021. arXiv: 2407.04747 [hep-ph].
- [29] G. Heinrich and J. Lang, “Renormalisation group effects in SMEFT for di-Higgs production,” Sep. 2024. arXiv: 2409.19578 [hep-ph].
- [30] L. Naterop and P. Stoffer, “Renormalization-group equations of the LEFT at two loops: dimension-five effects,” Dec. 2024. arXiv: 2412.13251 [hep-ph].
- [31] H. Béhusca-Maïto, A. Ilakovac, P. Kühler, M. Mador-Božinović and D. Stöckinger, “Two-loop application of the Breitenlohner-Maison/’t Hooft-Veltman scheme with non-anticommuting γ_5 : full renormalization and symmetry-restoring counterterms in an abelian chiral gauge theory,” *JHEP*, vol. 11, p. 159, 2021. DOI: 10.1007/JHEP11(2021)159. arXiv: 2109.11042 [hep-ph].

- [32] H. Béhusca-Maïto, “Renormalisation group equations for BRST-restored chiral theory in dimensional renormalisation: application to two-loop chiral-QED,” *JHEP*, vol. 03, p. 202, 2023. DOI: 10.1007/JHEP03(2023)202. arXiv: 2208.09006 [hep-th].
- [33] D. Stöckinger and M. Weißwange, “Full three-loop renormalisation of an abelian chiral gauge theory with non-anticommuting γ_5 in the BMHV scheme,” *JHEP*, vol. 02, p. 139, 2024. DOI: 10.1007/JHEP02(2024)139. arXiv: 2312.11291 [hep-ph].
- [34] P. Kühler and D. Stöckinger, “Two-Loop Renormalization of a Chiral $SU(2)$ Gauge Theory in Dimensional Regularization with Non-Anticommuting γ_5 ,” Apr. 2025. arXiv: 2504.06080 [hep-ph].
- [35] P. Kühler, D. Stöckinger and M. Weißwange, “Advances at the γ_5 -Frontier,” *PoS*, vol. LL2024, p. 022, 2024. DOI: 10.22323/1.467.0022. arXiv: 2407.07247 [hep-ph].
- [36] J. A. M. Vermaseren, “New features of FORM,” Oct. 2000. arXiv: math-ph/0010025.
- [37] B. Ruijl, T. Ueda and J. Vermaseren, “FORM version 4.2,” Jul. 2017. arXiv: 1707.06453 [hep-ph].
- [38] B. Ruijl *et al.* “FORM version 4.3.1 — Reference Manual.” (Apr. 2023), [Online]. Available: file:///home/matthias/Downloads/form-4.3.1-manual.pdf. (accessed: 21.10.2024).
- [39] P. Nogueira, “Automatic Feynman Graph Generation,” *J. Comput. Phys.*, vol. 105, pp. 279–289, 1993. DOI: 10.1006/jcph.1993.1074.
- [40] T. Luthe, “Fully massive vacuum integrals at 5 loops,” Ph.D. dissertation, Bielefeld U., 2015.
- [41] V. Maheria, “Semi- and Fully-Inclusive Phase-Space Integrals at Four Loops,” Ph.D. dissertation, Hamburg U., 2022.
- [42] A. V. Smirnov and F. S. Chuharev, “FIRE6: Feynman Integral REDuction with Modular Arithmetic,” *Comput. Phys. Commun.*, vol. 247, p. 106877, 2020. DOI: 10.1016/j.cpc.2019.106877. arXiv: 1901.07808 [hep-ph].
- [43] A. V. Smirnov and M. Zeng, “FIRE 6.5: Feynman integral reduction with new simplification library,” *Comput. Phys. Commun.*, vol. 302, p. 109261, 2024. DOI: 10.1016/j.cpc.2024.109261. arXiv: 2311.02370 [hep-ph].
- [44] A. von Manteuffel and C. Studerus, “Reduze 2 - Distributed Feynman Integral Reduction,” Jan. 2012. arXiv: 1201.4330 [hep-ph].
- [45] P. Maierhöfer, J. Usovitsch and P. Uwer, “Kira—A Feynman integral reduction program,” *Comput. Phys. Commun.*, vol. 230, pp. 99–112, 2018. DOI: 10.1016/j.cpc.2018.04.012. arXiv: 1705.05610 [hep-ph].
- [46] J. Klappert, F. Lange, P. Maierhöfer and J. Usovitsch, “Integral reduction with Kira 2.0 and finite field methods,” *Comput. Phys. Commun.*, vol. 266, p. 108024, 2021. DOI: 10.1016/j.cpc.2021.108024. arXiv: 2008.06494 [hep-ph].
- [47] J. Klappert and F. Lange, “Reconstructing rational functions with FireFly,” *Comput. Phys. Commun.*, vol. 247, p. 106951, 2020. DOI: 10.1016/j.cpc.2019.106951. arXiv: 1904.00009 [cs.SC].

- [48] J. Klappert, S. Y. Klein and F. Lange, “Interpolation of dense and sparse rational functions and other improvements in FireFly,” *Comput. Phys. Commun.*, vol. 264, p. 107968, 2021. DOI: 10.1016/j.cpc.2021.107968. arXiv: 2004.01463 [cs.MS].
- [49] A. von Manteuffel and R. M. Schabinger, “A novel approach to integration by parts reduction,” *Phys. Lett. B*, vol. 744, pp. 101–104, 2015. DOI: 10.1016/j.physletb.2015.03.029. arXiv: 1406.4513 [hep-ph].
- [50] A. von Manteuffel and R. M. Schabinger, “Quark and gluon form factors to four-loop order in QCD: the N_f^3 contributions,” *Phys. Rev. D*, vol. 95, no. 3, p. 034030, 2017. DOI: 10.1103/PhysRevD.95.034030. arXiv: 1611.00795 [hep-ph].
- [51] T. Peraro, “Scattering amplitudes over finite fields and multivariate functional reconstruction,” *JHEP*, vol. 12, p. 030, 2016. DOI: 10.1007/JHEP12(2016)030. arXiv: 1608.01902 [hep-ph].
- [52] Y. Schroder and A. Vuorinen, “High-precision epsilon expansions of single-mass-scale four-loop vacuum bubbles,” *JHEP*, vol. 06, p. 051, 2005. DOI: 10.1088/1126-6708/2005/06/051. arXiv: hep-ph/0503209.
- [53] S. P. Martin and D. G. Robertson, “Evaluation of the general 3-loop vacuum Feynman integral,” *Phys. Rev. D*, vol. 95, no. 1, p. 016008, 2017. DOI: 10.1103/PhysRevD.95.016008. arXiv: 1610.07720 [hep-ph].
- [54] M. Czakon, “The Four-loop QCD beta-function and anomalous dimensions,” *Nucl. Phys. B*, vol. 710, pp. 485–498, 2005. DOI: 10.1016/j.nuclphysb.2005.01.012. arXiv: hep-ph/0411261.
- [55] S. Wolfram, *Mathematica 12.0*, Published by Wolfram Research Inc., 2019. [Online]. Available: <https://www.wolfram.com>.
- [56] M. F. Zoller, “Four-loop QCD β -function with different fermion representations of the gauge group,” *JHEP*, vol. 10, p. 118, 2016. DOI: 10.1007/JHEP10(2016)118. arXiv: 1608.08982 [hep-ph].
- [57] K. G. Chetyrkin and M. F. Zoller, “Four-loop renormalization of QCD with a reducible fermion representation of the gauge group: anomalous dimensions and renormalization constants,” *JHEP*, vol. 06, p. 074, 2017. DOI: 10.1007/JHEP06(2017)074. arXiv: 1704.04209 [hep-ph].
- [58] F. Herzog, B. Ruijl, T. Ueda, J. A. M. Vermaseren and A. Vogt, “The five-loop beta function of Yang-Mills theory with fermions,” *JHEP*, vol. 02, p. 090, 2017. DOI: 10.1007/JHEP02(2017)090. arXiv: 1701.01404 [hep-ph].
- [59] T. Luthe, A. Maier, P. Marquard and Y. Schroder, “The five-loop Beta function for a general gauge group and anomalous dimensions beyond Feynman gauge,” *JHEP*, vol. 10, p. 166, 2017. DOI: 10.1007/JHEP10(2017)166. arXiv: 1709.07718 [hep-ph].
- [60] Z. Bern and A. G. Morgan, “Massive loop amplitudes from unitarity,” *Nucl. Phys. B*, vol. 467, pp. 479–509, 1996. DOI: 10.1016/0550-3213(96)00078-8. arXiv: hep-ph/9511336.
- [61] Z. Bern, A. De Freitas and L. J. Dixon, “Two loop helicity amplitudes for gluon-gluon scattering in QCD and supersymmetric Yang-Mills theory,” *JHEP*, vol. 03, p. 018, 2002. DOI: 10.1088/1126-6708/2002/03/018. arXiv: hep-ph/0201161.

- [62] M. Heller, A. von Manteuffel, R. M. Schabinger and H. Spiesberger, “Mixed EW-QCD two-loop amplitudes for $q\bar{q} \rightarrow \ell^+\ell^-$ and γ_5 scheme independence of multi-loop corrections,” *JHEP*, vol. 05, p. 213, 2021. DOI: 10.1007/JHEP05(2021)213. arXiv: 2012.05918 [hep-ph].
- [63] M. Misiak and M. Munz, “Two loop mixing of dimension five flavor changing operators,” *Phys. Lett. B*, vol. 344, pp. 308–318, 1995. DOI: 10.1016/0370-2693(94)01553-0. arXiv: hep-ph/9409454.
- [64] K. G. Chetyrkin, M. Misiak and M. Munz, “Beta functions and anomalous dimensions up to three loops,” *Nucl. Phys. B*, vol. 518, pp. 473–494, 1998. DOI: 10.1016/S0550-3213(98)00122-9. arXiv: hep-ph/9711266.
- [65] J.-N. Lang, S. Pozzorini, H. Zhang and M. F. Zoller, “Two-Loop Rational Terms in Yang-Mills Theories,” *JHEP*, vol. 10, p. 016, 2020. DOI: 10.1007/JHEP10(2020)016. arXiv: 2007.03713 [hep-ph].
- [66] B. Ruijl, F. Herzog, T. Ueda, J. A. M. Vermaseren and A. Vogt, “The R*-operation and five-loop calculations,” *PoS*, vol. RADCOR2017, p. 011, 2018. DOI: 10.22323/1.290.0011. arXiv: 1801.06084 [hep-ph].
- [67] C. Anastasiou, J. Karlen and M. Vicini, “Tensor reduction of loop integrals,” *JHEP*, vol. 12, p. 169, 2023. DOI: 10.1007/JHEP12(2023)169. arXiv: 2308.14701 [hep-ph].
- [68] J. Goode, F. Herzog, A. Kennedy, S. Teale and J. Vermaseren, “Tensor reduction for Feynman integrals with Lorentz and spinor indices,” *JHEP*, vol. 11, p. 123, 2024. DOI: 10.1007/JHEP11(2024)123. arXiv: 2408.05137 [hep-ph].
- [69] J. Goode, F. Herzog and S. Teale, “OPITeR: A program for tensor reduction of multi-loop Feynman Integrals,” Nov. 2024. arXiv: 2411.02233 [hep-ph].
- [70] D. Binosi, J. Collins, C. Kaufhold and L. Theussl, “JaxoDraw: A Graphical user interface for drawing Feynman diagrams. Version 2.0 release notes,” *Comput. Phys. Commun.*, vol. 180, pp. 1709–1715, 2009. DOI: 10.1016/j.cpc.2009.02.020. arXiv: 0811.4113 [hep-ph].